



1 **Picturing and modelling catchments by representative** 2 **hillslopes**

3 Ralf Loritz¹, Sibylle K. Hassler¹, Conrad Jackisch¹, Niklas Allrogen², Loes van Schaik³,
4 Jan Wienhöfer¹, and Erwin Zehe¹

5 ¹ Karlsruhe Institute of Technology (KIT), Institute of water and river basin management,
6 Karlsruhe, Germany

7 ² University of Potsdam, Institute of Earth and Environmental Science, Potsdam,
8 Germany

9 ³ Technische Universität Braunschweig, Environmental Systems Analysis, Institute of
10 Geocology, Braunschweig, Germany

11

12 *Correspondence to:* Ralf Loritz (Ralf.Loritz@kit.edu)

13

14 **Abstract:** Despite the numerous hydrological models existing in hydrology we are
15 limited to a few forms of conceptualization when abstracting hydrological systems into
16 different model frameworks. Speaking in black and white terms, in most cases
17 hydrological systems are either represented spatially lumped with conceptual models or
18 spatially explicit with physically-based models. Physically-based models are often
19 parameter-rich, making the parametrization challenging, while conceptual models are
20 parsimonious, with only a few parameters needing to be identified. But this simplistic
21 mathematical expression is often also their drawback since their model states and
22 parameters are difficult to translate to the physical properties of a catchment. It is
23 interesting to note that both hydrological modeling approaches often start with the
24 drawing of a perceptual model. This follows the hydrologist's philosophy to separate
25 dominant patterns and processes from idiosyncratic system details. Due to the importance
26 of hillslopes as key landscape elements perceptual models are often displayed as 2D
27 cross-sections. In this study we examine whether we can step beyond the qualitative
28 character of perceptual models by using them as blueprint for setting up representative
29 hillslope models. Thereby we test the hypothesis if a single hillslope can represent the
30 functioning of an entire lower mesoscale catchment in a spatially aggregated way. We do
31 this by setting up and testing two hillslope models in catchments located in two different
32 geological settings, Schist and Marl, using a two-dimensional physically-based model.
33 Both models are parametrized based on intensive field data and literature values without



34 automatic calibration. Remarkably we are able to not only match the water balance of
35 both catchments but further have some success in simulating runoff generation as well as
36 soil moisture and sap flow dynamics. Particularly, our findings demonstrate that both
37 models performed well during the winter season and clearly worse during the summer
38 period. Virtual experiments revealed that this was most likely either due to a poor
39 representation of the onset of vegetation in the Schist catchment or due to emergence of
40 soil cracks in the Marl area. Both findings underpin that a static parameterization of
41 hydrological models might be problematical in case of emergent behavior. Additional
42 virtual experiments indicate that the storage of water in the bedrock and not so much the
43 topographic gradient is a first order control on the hydrological functioning of the Schist
44 catchment. We conclude that the representative hillslope concept is a feasible approach in
45 data rich regions and that this form of abstraction provides an added value to the
46 established conceptualization frameworks in hydrology.



47 **1 Introduction**

48 **1.1 Representative hillslope models as catchment pictures**

49 According to Heidegger (1977), “the modern is characterized as the age of the world
50 picture”. Science conceives and grasps the world as a picture rather than simply picturing
51 the world. In hydrology such a picture is for instance reflected by a perceptual model.
52 Perceptual models are abstractions of a hydrological system displaying how dominant
53 properties and processes jointly control its functioning. It is conspicuous that these
54 models are frequently drawn in the form of a hillslope-like cross-section. This reflect that
55 hillslopes are often regarded as the key landscape elements controlling transformation of
56 precipitation and radiation inputs into terrestrial fluxes and stocks of water (e.g. Bronstert
57 and Plate, 1997), energy (Zehe et al., 2010a, 2013) and sediments (Mueller et al., 2010).
58 Although any perceptual model is a simplification and is pre-determined by the
59 designer’s background and experience (Beven, 2012) it provides a useful means to
60 facilitate communication between researchers with different backgrounds by integrating
61 their knowledge (Seibert and McDonnell, 2002). Further, perceptual models are the
62 natural starting point for any process-oriented model exercise.

63 Due to their simplistic way of abstracting the landscape, the rationale of this study is to
64 explore whether perceptual models of two distinctly different catchments, derived from
65 comprehensive and diverse field observations, may serve as blueprints for setting up
66 representative hillslope models. Recently, Wrede et al. (2015) followed the same idea by
67 deriving conceptual model structures from perceptual models of three headwaters located
68 in the Attert experimental basin, which is also our study area. However, here we use a
69 physically-based model because the underlying equations depend on observable
70 parameters and state variables (Loague and VanderKwaak, 2004; Zehe et al., 2006). The
71 representative hillslope model is hence a straightforward conceptualization of the
72 underlying perceptual model (as illustrated in Figure 3, section 2) by drawing from
73 available field data and expert knowledge. We regard this as the most parsimonious
74 representation of the catchment in a physically-based model framework which provides a
75 spatially explicit but yet effective picture about how gradients, spatial patterns of soil
76 properties and rapid flow paths jointly control the dominant processes. Testing of such an
77 approach offers several avenues for scientific learning as further specified below.

78



79 The usefulness of physically-based models as learning tools has been corroborated in
80 several studies, especially those working on the hillslope and lower catchment mesoscale.
81 For instance Hopp and McDonnell (2009) explored the role of bedrock topography on the
82 runoff formation. Complementary to this, Bishop et al. (2015), Wienhöfer and Zehe
83 (2014) and Klaus and Zehe (2011) focused on the influence of lateral and vertical
84 preferential flow networks on subsurface water flow and solute transport, including the
85 issue of equifinality and its reduction. These and other studies (e.g. Ebel et al., 2008)
86 corroborate that physically-based models may be benchmarked against a variety of
87 observations beyond stream flow – such as soil moisture observations, groundwater tables
88 or tracer break-through curves. Essentially, such a multi-response evaluation reveals
89 whether a model allows consistent predictions of dynamics within the catchment and for
90 its integral response behavior (Ebel and Loague, 2006). Last but not least, virtual
91 experiments with physically-based models are straightforward to implement and interpret,
92 because their parameters and their spatial setup are well connected to those observables
93 we use to characterize hydrological systems. Such virtual experiments may reveal first
94 order controls on hydrological system behaviors, and thereby sustain scientific learning
95 (Weiler and McDonnell, 2004), for instance to decide which variables shall be observed
96 within field campaigns in order to reduce equifinality (Zehe et al., 2014) as further
97 specified below.

98 **1.2 Challenges in modeling catchments by representative hillslopes**

99 Several physically-based and distributed model studies employ typical hillslope catenas
100 as building blocks (Bronstert and Plate, 1997; Zehe and Blöschl, 2004; Jackisch et al.,
101 2014). However, the challenge of how to identify a behavioral representative hillslope as
102 most parsimonious representation of a small catchment in a physically-based model has
103 rarely been addressed. This reflects the fact that the identifiability of representative
104 hillslopes has been strongly questioned since the idea was born. For example, Beven
105 (2006) argues that neither the hillslope form is uniquely defined nor is it clear whether it
106 is the form that matters, the pattern of saturated areas (Dunne and Black, 1970) or the
107 subsurface architecture. The enormous spatial variability of soil hydraulic properties and
108 preferential flow paths in conjunction with process non-linearity are additional arguments
109 against the identifiability of representative hillslope models (Beven and Germann, 2013).
110 However, hillslopes act as miniature catchments (Bachmair and Weiler, 2011), which
111 made Zehe et al. (2014) postulate that structurally similar hillslopes act as functional units



112 for the runoff generation and might thereby be a key unit for understanding functional
113 behavior of catchments of organized complexity (Dooge, 1986). Complementarily,
114 Robinson et al. (1995) showed that the behavior of catchments up to the lower mesoscale
115 are still strongly dominated by the hillslope behavior. Kirkby (1976) showed for
116 catchments extending up to 50 km² that random river networks had the same explanative
117 power for catchment behavior as the real river network. He concluded that as long as river
118 networks are not dominant the anomalous areas of the catchment bear the key to
119 understand its functioning. Unfortunately, topographic characteristics are not always
120 conclusive for explaining differences in hydrological behavior, as recently shown by
121 Jackisch (2015) for headwaters located in distinctly different geological parts of the Attert
122 experimental basin.

123

124 We hence suggest that it is worth investigating to what extent the behavior of these lower
125 mesoscale catchments can be explained using a single representative hillslope model. In
126 line with the arguments stated above such a representative hillslope can be neither a one-
127 to-one copy of a real hillslope in a catchment nor a simple average of several hillslopes
128 and their structural properties. A much more promising avenue might be to conceptualize
129 the representative hillslope as a functional analogue of the perceptual model, which is in
130 turn a generalized and simplified picture of the catchment structure and functioning. The
131 challenge in this model identification process is to balance necessary complexity with
132 greatest possible simplicity by preserving the typical patterns and structural catchment
133 characteristics and to neglect the unnecessary or idiosyncratic ones (Zehe et al., 2014).
134 Naturally, it has to be expected that a representative hillslope is, as a spatially aggregated
135 two-dimensional model of a catchment, not uniquely identifiable because non-uniqueness
136 and equifinality is inherent to all of the governing equations (Kirchner, 2006; Klaus and
137 Zehe, 2010; Zehe et al. 2014). But the degrees of freedom in the identification of
138 behavioral physically model structures can be reduced by using complementary
139 observations such as tracers (Klaus and Zehe 2011, Wienhöfer and Zehe, 2014) or
140 constraining parameters based on observations (Bárdossy, 2006).

141

142 Other reasons why representative hillslope studies are rarely realized are the challenges
143 and data needs that go along with applying physically-based models in larger
144 heterogeneous environmental systems (e.g. Or et al., 2015) as well as the vital debate
145 about their limitations. Physically-based models typically rely on the Darcy-Richards



146 concept for simulating soil water dynamics, the Penman–Monteith equation for
147 simulating soil-vegetation-atmosphere exchange processes and 1-D or 2-D hydraulic
148 approaches for simulating overland and stream flow. Each of these concepts is naturally
149 subject to the limitations arising from our imperfect understanding of the related (bio-)
150 physical processes and the limited transferability of process descriptions which were
151 derived under idealized laboratory conditions to settings in natural systems (Grayson et
152 al., 1992; Gupta et al., 2012). For example, the Darcy-Richards equation assumes
153 dominance of capillarity controlled, mainly diffusive soil water fluxes and local
154 thermodynamic equilibrium conditions. While these assumption are well justified when
155 the radiation balance controls soil water dynamics it is violated during rainfall events
156 which trigger preferential flow (Hassanizadeh 2002; Simunek et al. 2003; Or 2008). The
157 variety of concepts that have been proposed to incorporate not-well mixed preferential
158 flow into hydrological models ranges from early stochastic convection (Simmons 1982),
159 double-domain approaches (Haws et al., 2005, Köhne et al., 2006, Bishop et al., 2015),
160 spatially explicit representations of macropores as connected flow paths (Sander and
161 Gerke 2009, Klaus and Zehe, 2010) to pore network models (Vogel and Roth, 2001;
162 Bastardie et al., 2003; Katuwal et al., 2015). As each of these approaches has specific
163 advantages and drawbacks we still lack an approach that is commonly agreed upon for
164 studies at the hillslope scale (Beven and Germann, 2013).

165

166 But besides the widely discussed limitations of hydrological models to represent
167 preferential flow, the simulation of soil-vegetation-atmosphere transfer is likely to be an
168 even weaker point. The large number of stomata conductance models that have been
169 proposed (Damour et al., 2010) reflects the uncertainty in the community on how to
170 represent plant physiological controls on transpiration in hydrological and land surface
171 models. Also a proper representation of the vegetation phenology is a challenge for
172 hydrological modelling. Most physically based models account for dynamic changes in
173 leaf area index, root depth and plant cover, however, often in the form of fixed annual
174 cycles that have been derived at a specific catchment or are taken from the literature. Soil
175 water is, however, a limiting factor for growth of agricultural crops (Abrahamsen and
176 Hansen, 2000; Kucharik and Brye, 2003) and the dynamics of functional vegetation,
177 particularly in semi-arid areas (e.g. Rodriguez-Iturbe, 1999; Tietjen and Jeltsch, 2007;
178 Tietjen et al., 2010). This implies that the plant phenology should be more of a dynamic
179 state of the model rather than a parameter set with a fixed annual cycle (Jackisch et al.,



180 2014). In those cases where locally observed time series of phenological data and crop
181 growth are not available, we often rely on parameterizations from the literature. While a
182 transfer of such parameter setups might not impair the simulation of direct runoff reaction
183 on the event scale, it may create serious biases in simulated soil moisture dynamics (Zehe
184 et al., 2010a) and long term simulations of the water balance of a catchment.

185 Because of the mentioned shortcomings, simulations with physically-based models will
186 essentially bear the fingerprints of the bio-physical limitations of the underlying equations
187 and of the limited transferability of parameter sets among places (Beven, 2002).
188 However, these limitations should not be misinterpreted as an argument against applying
189 imperfect physically-based models but rather as a challenge and an option for learning
190 (Loague and VanderKwaak, 2004). Particularly so, since the identification of these
191 limitations itself is of key importance to separate the predictable from the un-predictable
192 as well as for improving theoretical underpinnings of hydrological models (Clark et al.,
193 2016).

194 **1.3 Objectives and approach**

195 Despite - or in fact because of - all the shortcomings and possibilities discussed above, we
196 explore if and how we can picture and model two lower mesoscale catchments in the
197 Attert experimental basin by representative hillslopes. The rationale of our study is not to
198 “sell” a particular model, but a) to shed light on to what extent this most parsimonious
199 representation of the dominant catchment structural properties in a physically-based
200 model allows behavioral simulations of catchment functioning beyond reproduction of
201 stream flow and b) to identify limits in our theories and related physically-based models
202 by analyzing the model deficiencies as proposed by Ebel and Loague (2006). We hence
203 avoid automatic parameter calibration to optimize curve fitting since there are more
204 parsimonious and better suited model structures for this purpose. We instead rely on
205 various available observations, process-based reasoning, and appropriate literature data
206 for conceiving perceptual models and parameterizing representative hillslope models as
207 their functional analogues. More specifically, we use geophysical images to constrain
208 subsurface strata and bedrock topography (as suggested by e.g. Graeff et al., 2009),
209 representative soil-water retention curves derived from a large data set of undisturbed soil
210 samples, soil pits and dye staining experiments, and predefined phenological data (Zehe
211 et al., 2001) for model parametrization.

212



213 The key challenge in the hillslope identification process is to achieve the right balance of
214 complexity and simplicity by finding patterns and dominant structures in the
215 overwhelming heterogeneity of the surface and subsurface. By aggregating a catchment in
216 a two-dimensional hillslope and by choosing CATFLOW (described in detail in section
217 2.3) as the model framework we essentially assume:

- 218 • That the spatial organization of the catchment creates anisotropy in the fluxes
219 sustaining the water balance and stream flow production which allows an
220 aggregated description in two dimensions, representing downslope and vertical
221 flows as well as the dominant gradients, hydraulic properties and flow paths in
222 spatially explicit but yet effective manner.
- 223 • Timing of streamflow is mainly controlled by the hillslope properties, which
224 implies that the time scale of lateral flow concentration in the hillslope body is
225 larger than the time scale of flood routing in the river network at this scale.
- 226 • An effective representation of the topology of preferential flow paths is more
227 important than a representation of non-equilibrium between rapid flow and matrix
228 flow at this scale;
- 229 • An effective soil water retention curve derived from a large data set of
230 undisturbed soil samples is sufficient for simulation of the fluxes and average
231 storage dynamics controlling the water balance and stream flow production. The
232 relevant heterogeneity arises from spatial variability in the saturated hydraulic
233 conductivity and porosity, which may be accounted for in stochastic form.

234
235 Finally we benchmark the hillslope models, after successful reproduction of the water
236 balance, against the hydrograph as well as distributed soil moisture and sap flow
237 observations. This exercise will reveal the validity of the listed assumptions and of our
238 notion of the “perfect” balance of complexity and simplicity, as well as whether the
239 parameterization of a representative hillslope is transferable to a different catchment in
240 the same landscape and time. It can be furthermore seen as a first test of the concept of
241 hillslope scale functional units which constrain similarity of runoff production (Zehe et
242 al., 2014). We hence perform several virtual experiments to a) identify first order controls
243 on the functioning of these “functional units” and guide future field campaigns for their
244 identification and b) find key gaps in available process representations in order to sharpen
245 questions for future research.



246 **2. Study site and data basis**

247 **2.1 The Attert experimental basin**

248 This study is based on comprehensive laboratory and field data collected in the Attert
249 basin within the CAOS (Catchments As Organized Systems) research unit (Figure 1,
250 Zehe et al., 2014). The Attert basin is located in the mid-western part of the Grand-Duchy
251 of Luxembourg and has a total area of 288 km². Mean monthly temperatures range from
252 18°C in July to a minimum of 0°C in January while mean annual precipitation in the
253 catchment varies around 850 mm (1971–2000) (Pfister et al., 2000). The catchment
254 covers three geological formations, the Devonian schists of the Ardennes massif in the
255 northwest, Triassic sandy marls in the center and a small area of Luxemburg sandstone
256 (Jurassic) in the southern part of the catchment (Martínez-Carreras et al., 2012). Our
257 study areas are headwaters named Colpach in the Schist area (19.4 km²) and Wollefsbach
258 in the Marl area (4.5 km²). As both catchments are located in distinctly different
259 geologies (Figure 1) and land use settings, they differ considerably with respect to runoff
260 generation and the dominant controls (e.g. Bos et al. 1996, Martínez-Carreras et al. 2012,
261 Fenicia et al. 2014, Wrede et al. 2015 and Jackisch 2015).

262 **2.1.1 Colpach catchment: perceptual model of structure and functioning**

263 The Colpach catchment has a total area of 19.4 km² and an elevation range between 265
264 to 512 m a.s.l. It is situated in the northern part of the Attert basin on the Devonian schists
265 of the Ardennes massif. Around 65 % of the catchment, mainly the steep hillslopes, are
266 forested (Figure 2). In contrast, the plateaus at the hill tops are predominantly used for
267 agriculture and pasture. Several geophysical experiments and drillings showed that
268 bedrock and surface topography are distinctly different. The bedrock is undulating and
269 rough with ridges, depressions and cracks (compare perceptual model Figure 3 A and
270 also ERT image in Figure 6 B). Depressions in the bedrock interface are filled with
271 weathered, silty materials which may form local pools and reservoirs with a high water
272 holding capacity. These features are particularly important since lateral water flow along
273 the bedrock interface is the dominant runoff process (Wrede et al., 2015). Specifically the
274 subsurface structure is deemed to cause typical threshold-like runoff behavior similar to
275 the fill-and-spill mechanism proposed by Tromp-Van Meerveld & McDonnell (2006).
276 Further indication that fill-and-spill is a dominant process is given by the fact that the
277 parent rock is reported as impermeable, which makes deep percolation through shallower



278 un-weathered schist layers into a large groundwater body unlikely (Juilleret et al., 2011).
279 The lack of significant observations of base flow underpins this notion. Furthermore,
280 surface runoff has been rarely observed in the catchment, except along forest roads,
281 which suggests a high infiltrability of the prevailing soils (Bos et al., 1996). This is in line
282 with distributed permeameter measurements and soil sampling performed by Jackisch
283 (2015). Moreover, numerous irrigation and dye staining experiments highlight the
284 important role of vertical structures for rapid infiltration and subsequent subsurface runoff
285 formation (Jackisch (2015), Figure 2 B).

286 **2.1.2 Wollefsbach catchment: perceptual model of structure and functioning**

287 The Wollefsbach catchment is located in the Triassic sandy marls formation of the Attert
288 basin. It has a size of 4.5 km² and low topographic gradients, with 61 m of maximum
289 elevation difference resulting in gentle slopes covering altitudes between 245 to 306 m
290 a.s.l. The catchment is intensively used for agriculture and pasture and only around 7 %
291 are forested (Figure 2 C) and hillslope are often tile drained (compare perceptual model
292 sketch in Figure 3 B). The marly soils are highly heterogeneous, from sandy loams to
293 thick clay lenses. Generally they are very silty with high water holding capacities and
294 mostly low saturated hydraulic conductivity of the soil matrix. Similar to the Colpach
295 catchment, vertical preferential flow paths play a major role for the runoff generation;
296 their origin, however, is distinctly different between the seasons. Biopores are dominant
297 in spring and autumn due to the high abundance of earthworms. Because earthworms are
298 dormant during midsummer and winter, their burrows are partly disconnected by
299 ploughing, shrinking and swelling of the soils (Figure 2 D, see also Figure 4). At the same
300 time, soil cracks emerge during long dry spells in midsummer due to the considerable
301 amount of smectite clay minerals in these soils, which drastically increase soil
302 infiltrability in summer (Zehe et al. 2007, Figure 4). The seasonally varying interaction of
303 both types of preferential flow paths with a dense man-made subsurface drainage network
304 is probably the reason for the flashy runoff regime of this catchment, where discharge
305 drops rapidly to baseflow when precipitation events end. However, as the exact position
306 of the subsurface drainage network and the worm burrows as well as the threshold for soil
307 crack emergence are unknown, the specific influence of each structure on runoff
308 generation is difficult to estimate.



309 **2.1.3 Water balance and seasonality**

310 The water balance of the Colpach and Wollefsbach catchments for several hydrological
311 years, presented as normalized double mass curves, are shown in Figure 5. Normalized
312 double mass curves are well suited for describing the annual water balance of a catchment
313 because they relate the cumulated runoff to the cumulated precipitation both divided by
314 the sum of the annual precipitation. Annual runoff coefficients in the Colpach catchment
315 vary around 0.51 ± 0.06 within the four hydrological years (Figure 5 A). In the
316 Wollefsbach catchment the annual runoff coefficients are smaller than in the Colpach
317 catchment and vary across a wider range, from 0.26 to 0.46 (Figure 5 B). In both
318 catchments the winter period is characterized by step-like changes which reflect fast
319 water mobilization during rainfall events partly due to rapid subsurface flow. In contrast,
320 the summer regime in the vegetation period is characterized by a smooth and almost flat
321 line. Accumulated rainfall input is not transformed into additional runoff but
322 predominantly into evapotranspiration (Jackisch 2015). Additionally we used a
323 temperature index model from Menzel et al., (2003) to detect the onset of the vegetation
324 period and to separate the vegetation-controlled summer regime from the winter period
325 which was already successfully used by Seibert et al. (2016) to mark onset and duration
326 on the summer regime in 22 catchments of the Bavarian Danube basin.

327 **2.2 Data basis**

328 **2.2.1 Surface topography and land use**

329 Topographic analyses are based on a 5 m LIDAR digital elevation model which was
330 aggregated and smoothed to 10 m resolution. Land use data from the “Occupation
331 Biophysic du Sol” is based on CORINE land use classes analyzed by colour infrared areal
332 images which were generated in 1999 from the “Administration du cadaster et de la
333 Topographie” at a scale of 1:15000.

334 **2.2.2 Subsurface structure and bedrock topography**

335 We used hillslope scale 2D electrical resistivity tomography (ERT) in combination with
336 augers and soil pits to estimate bedrock topography in the Schist area. Our auger profiles
337 revealed, in line with Juilleret et al., (2011) and Wrede et al., (2015), that the vertical soil
338 setup comprises a weathered silty soil layer with a downwards increasing fraction of rock
339 fragments, which is underlain by a transition zone of weathered bedrock fragments



340 followed by non-weathered and impermeable bedrock. Spatial subsurface information of
341 representative hillslopes were obtained from 2D ERT sections collected using a GeoTom
342 (GeoLog) device at four profiles on two hillslopes in the Colpach catchment. We used a
343 Wenner configuration with electrode spacing of 0.5 m and 25 depth levels: electrode
344 positions were recorded at a sub-centimeter accuracy using a total station providing 3D
345 position information. Application of a robust inversion scheme as implemented in
346 Res2Dinv (Loke, 2003) resulted in two-layered subsurface resistivity model Figure 6 B.
347 The upper 1 - 3 m are characterized by high resistivity values larger than $1500 \Omega \cdot \text{m}$. This
348 is underlain by a layer of generally lower resistivity values smaller than $1500 \Omega \cdot \text{m}$. In
349 line with the study of (Wrede et al., 2015) and in correspondence with the maximum
350 depth of the local auger profiles, we interpreted the transition from high to low resistivity
351 values to reflect the transition zone between bedrock and unconsolidated soil. In
352 consequence, we regard the $1500 \Omega \text{m}$ isoline as being representative for the soil-bedrock
353 interface.

354 **2.2.3 Soil hydraulic properties and infiltrability**

355 We determined soil texture, saturated hydraulic conductivity and the soil water retention
356 curve for 51 soil samples in the Schist area and 28 in the Marl area. Saturated hydraulic
357 conductivity was measured with undisturbed 250 ml ring samples with the KSAT
358 apparatus (UMS GmbH). The apparatus records the falling head of the water supply
359 through a highly sensitive pressure transducer which is used to calculate the flux. The soil
360 water retention curve of the drying branch was measured with the same samples in the
361 HYPROP apparatus (UMS GmbH) and subsequently in the WP4C dew point hygrometer
362 (Decagon Devices Inc.). The HYPROP records total mass and matric head in two depths
363 in the sample over some days when it was exposed to free evaporation (Peters and
364 Durner, 2008, Jackisch 2015 for further details). For both geological settings we
365 estimated a mean soil retention curve by grouping the observation points of all soil
366 samples (51 and 28, respectively), and averaging them in steps of 0.05 pF. We then fitted
367 a van Genuchten-Mualem model using a maximum likelihood method to these averaged
368 values (Table 1 and Figure 7).

369 **2.2.4 Meteorological forcing and discharge**

370 Meteorological data are based on observations from two official meteorological stations
371 (Useldange and Roodt) from the Administration des services techniques de l'agriculture



372 Luxembourg (ASTA). Air temperature, relative humidity, wind speed and global
373 radiation are provided on a temporal resolution of 1 h while precipitation data have a
374 temporal interval of 5 min. Precipitation was intensively quality checked by six
375 distrometers which are stationed within the Attert basin and by several randomly selected
376 rainfall events against rain radar observations, both by visual inspection. Discharge
377 observations are provided from the Luxembourg Institute of Science and Technology
378 (LIST).

379 **2.2.5 Sap flow, soil moisture data and meteorological forcing**

380 The Attert basin is instrumented with 45 automated sensor clusters. A single sensor
381 cluster measures rainfall, and soil moisture in three profiles with sensors in various
382 depths. In this study we use 38 soil moisture sensors located in the Schist area and 28
383 sensors located in the Marl area in 10 and 50 cm depth. The measurements (sensors
384 Decagon 5TE) have a temporal resolution of 5 min and an accuracy of ± 3 % volumetric
385 water content (VWC) with a resolution of 0.08 % VWC. Furthermore we use sap flow
386 measurements based on the heat ratio method (Burgess et al., 2001) at 61 trees at a
387 temporal resolution of 12 h- means. Selected trees are either European Beech or Oak
388 trees.

389 **2.3 The physically based model CATFLOW**

390 Model simulations were performed using the physically-based hydrological model
391 CATFLOW (Maurer, 1997; Zehe et al., 2001). The model has been successfully used and
392 specified in numerous studies (e.g. Zehe et al., 2005; Zehe et al. 2010; Wienhöfer and
393 Zehe, 2014; Zehe et al., 2014). The basic modelling unit is a two-dimensional hillslope.
394 The hillslope profile is discretized by curvilinear orthogonal coordinates in vertical and
395 downslope directions; the third dimension is represented via a variable width of the slope
396 perpendicular to the slope line at each node. Soil water dynamics are simulated based on
397 the Richards equation in the pressure based form and numerically solved using an implicit
398 mass conservative “Picard iteration” (Celia et al., 1990). The model can simulate
399 unsaturated and saturated subsurface flow and has hence no separate groundwater routine.
400 Soil hydraulic functions after van Genuchten-Mualem are mostly used, though several
401 other parameterizations are possible. Overland flow is simulated using the diffusion wave
402 approximation of the Saint-Venant equation and explicit upstreaming. The hillslope
403 module can simulate infiltration excess runoff, saturation excess runoff, re-infiltration of



404 surface runoff, lateral water flow in the subsurface as well as return flow. For catchment
405 modelling several hillslopes can be interconnected by a river network for collecting and
406 routing their runoff contributions, i.e. surface runoff or subsurface flow leaving the
407 hillslope, to the catchment outlet.

408 **2.3.1 Evaporation controls, root water uptake and vegetation phenology**

409 Soil evaporation, plant transpiration and evaporation from the interception store is
410 simulated based on the Penman–Monteith equation. Soil moisture dependence of the soil
411 albedo is also accounted for as specified in Zehe et al., (2001). Annual cycles of plant
412 phenological parameters, plant albedo and plant roughness are accounted for in the form
413 of tabulated data derived within the Weiherbach project (Zehe et al., 2001). Optionally,
414 the impact of local topography on wind speed and on radiation may be considered, if
415 respective data are available. The atmospheric resistance is equal to wind speed in the
416 boundary layer over the squared friction velocity u^* [$L T^{-1}$]. The former depends on
417 observed wind speed, plant roughness and thus plant height. The friction velocity depends
418 on observed wind speed as well as atmospheric stability, which is represented through six
419 stability classes depending on prevailing global radiation, air temperature and humidity.
420 The canopy resistance is the product of leaf area index and leaf resistance, which in turn
421 depends on stomata and cuticular resistance. The stomata resistance varies around a
422 minimum value, which depends on the Julian day as well as on a function of air
423 temperature, water availability in the root zone, the water vapour saturation deficit and
424 photosynthetic active radiation (Jarvis, (1976)). The soil conductance depends mainly on
425 the thickness of a topsoil layer controlling water vapour transport which is divided by the
426 water vapour diffusivity in soil. Root extraction is accounted for as a sink term that
427 operates as a flux per volume during potential evapotranspiration; the transpired water
428 is extracted uniformly along the entire root depth. When soil water content in the root
429 zone drops below a certain threshold root water uptake is controlled by the difference in
430 matric and root water potentials.

431 **2.3.2 Generation of rapid vertical and lateral flow paths**

432 Vertical and lateral preferential flow paths are represented as connected flow paths
433 containing an artificial porous medium with high hydraulic conductivity and very low
434 retention properties. This approach has also been followed by others (Nieber and Warner
435 1991; Castiglione et al. 2003; Lamy et al. 2009; Nieber and Sidle 2010), and was proven



436 to be suitable to predict hillslope scale preferential flow and tracer transport in the
437 Weiherbach catchment, a drained and agriculture dominated site in Germany (Klaus and
438 Zehe, 2011) and at the Heumöser hillslope, a forested site with fine textured marly soils
439 in Austria (Wienhöfer and Zehe, 2014). A Poisson process allocates the starting points of
440 the vertical structures sequentially along the soil surface and stepwise extends the vertical
441 preferential pathways downwards to their depth, while allowing for a lateral step with a
442 probability of typically 0.05 to 0.1 to establish tortuosity. Lateral preferential flow paths
443 to represent either pipes at the bedrock interface or the tile drains are generated in the
444 same manner: starting at the interface to the stream and stepwise extending them upslope,
445 again with a small probability for a vertical upward or downwards step to allow for a
446 tortuosity.

447 **3. Parametrization of the representative hillslope models**

448 **3.1 Colpach catchment**

449 *Surface topography, spatial discretization and land use*

450 We selected a real hillslope profile with a length of 350 m, a maximal elevation above the
451 stream of 54 m and a total area of 42600 m², which represents the average elevation
452 difference and lengths of all delineated 241 hillslopes in the Colpach catchment (Figure 6
453 A). The hillslope was discretized with a 1 m grid size in the downslope and 0.1 m grid
454 size in the vertical direction down to the depth of 2 m (Figure 3C). Land use was set to
455 mixed forest for the entire hillslope since forest covers 65 % of the catchment area,
456 especially the steeper hillslopes (Figure 3). Due to the absence of local data on the plant
457 phenological cycle we used fixed tabulated data characterizing the annual cycle of leaf
458 area index, ground cover, root depth, plant height, minimum stomata resistance and plant
459 roughness (Manning's n) derived within the study of Zehe et al., (2001) for the
460 Weiherbach catchment. We are aware that particularly the onset of the vegetation phase
461 depends strongly on the local climate setting. As such, this assumption may be reflected
462 in model bias during this period of the year; we explore the sensitivity of model results
463 for an improved estimate of the start of the vegetation period within the virtual
464 experiment 3. Boundary conditions were set to atmospheric boundary at the top, no flow
465 boundary at the right margin, free outflow boundary condition at the left boundary and a
466 gravitational flow boundary condition at the lower boundary. We used spin-up runs with



467 initial states of 70 % of saturation for the entire hydrological year of interest and used the
468 final soil moisture pattern for model initialization.

469

470 *Bedrock-topography and permeability, rapid subsurface flow paths and soil hydraulic*
471 *functions*

472 The shape of the bedrock interface was extracted from the ERT image based on the 1500
473 Ω/m contour line (Figure 6 B and Figure 3c). As a result, the soil depths in the hillslope
474 varied between 1 m to 1.8 m with local depressions that form water holding pools. Since
475 no quantitative data on bedrock permeability are available we use the relative
476 impermeable bedrock parametrization of Wienhöfer and Zehe (2014) but increased the
477 bedrock porosity from 0.35 to 0.4 to account for storage in fractures and cracks (Table 1).
478 The silty soil above the bedrock was characterized by the representative hydraulic
479 parameters obtained from field samples listed in Table 1. Macropore depths were drawn
480 from a normal distribution with mean 1 m and standard deviation 0.3 m in agreement with
481 the reported mean soil depth and dye staining experiments. Additionally, macropores
482 were slightly tortuous with a probability for a lateral step of 5 %. Conductivity of vertical
483 macropores was set to $5 \times 10^{-2} \text{ m s}^{-1}$, which corresponds well with the observation for
484 earthworm burrows (Shipitalo and Butt, 1999). Weathered Schist at the soil–bedrock
485 interface was represented by a 0.2 m thick layer using the parameter of the macropore
486 medium from Wienhöfer and Zehe, (2014; Table 1). Stochastic heterogeneity of soil
487 hydraulic properties was accounted for by perturbing the saturated hydraulic conductivity
488 with multiples generated with a two dimensional turning band generator (Zehe et al.
489 2010a). As proposed in (Zehe et al., 2010b) we used a rather short range of 5 m and a
490 nugget to sill ratio of 0.75.

491 **3.2 Wollefsbach catchment**

492 *Surface topography, spatial discretization and land use*

493 Topography and land use is much more uniform in the Wollefsbach compared to the
494 Colpach. We again selected a hillslope with an area of 373600 m², which is 853 m long
495 and has a maximal elevation of 53 m above the river. The hillslope was discretized into
496 550 horizontal and 20 vertical elements with an overall hillslope thickness of 2 m (Figure
497 3 D). The vertical grid size was in general set to 0.1 m while grid size in downslope
498 direction varied between 0.1 m within and close to the rapid flow path and 2 m within
499 reaches without macropores (Figure 3). Land use was divided into grassland within the



500 steeper and lower part of the hillslope and, after 425 m from the creek, to corn cultivation.
501 This configuration reflects well the typical land use pattern in the catchment. Due to the
502 absence of local data we used fixed tabulated data characterizing grassland and corn
503 derived within the Weiherbach catchment (Zehe et al., 2001).

504

505 *Bedrock-topography and permeability, rapid subsurface flow paths and soil hydraulic*
506 *functions*

507 Contrary to the Colpach, geophysical measurements and augers revealed bedrock and
508 surface as being more or less parallel. Soil depth was set to constant 1 m and the soil was
509 parameterized using the representative soil retention curves shown in Figure 7. Marly
510 bedrock was again parameterized according to values Wienhöfer & Zehe (2014) proposed
511 for the marly bedrock at the Heumöser hillslope (Table 1). Because of the vertical and
512 lateral drainage structures in the catchment we generated a rather dense network of
513 vertical fast flow path with the structure generator, which were partly connected to a 10
514 cm thick tile drain. The latter was generated in the standard depth of 80 cm assuming that
515 it extended 400 m upslope originating from the hillslope creek interface. The position of
516 macropores was selected with a Poisson process along the soil surface with a minimum
517 distance of 3 m. Vertical flow path and the pipe were parametrized using an artificial
518 porous medium (Table 1) proposed by Wienhöfer and Zehe, (2014). Boundary conditions
519 were set to atmospheric boundary at the top, no flow boundary at the right margin and a
520 free outflow boundary condition and a gravitational flow boundary condition were
521 prescribed at the left boundary and the lower boundary. The model was initialized in the
522 same manner as described for the Colpach.

523 **3.3 Model benchmarking**

524 Both reference hillslopes (A1 reference model Colpach; A2 reference model
525 Wollefsbach) were set up to reproduce the normalized double mass curves in both
526 catchments of the hydrological year 2014 within which a few test simulations were
527 judged using the Kling-Gupta efficiency (KGE) (Gupta et al. 2009). In the next step we
528 compared the sum of simulated overland flow, subsurface storm flow across the right
529 hillslope boundary and deep percolation across the bottom boundary to observed stream
530 flow hydrograph, both visually and also based on the KGE, the Nash-Sutcliffe efficiency
531 (NSE) and the logarithmic NSE (log NSE). Furthermore, we validated the model setups



532 without any tuning against available soil moisture observations as well as against sap
533 flow velocities observed in the in the Colpach.

534 **3.3.1 Virtual experiments**

535 We performed three virtual experiments in the Colpach by changing surface and bedrock
536 topography as well as plant physiological cycles to explore first-order controls on the
537 water balance and the relative importance of the underlying observations. Additionally,
538 we performed a virtual experiment in the Wollefsbach by increasing the hydraulic
539 conductivity of the soils in the summer months to account for the effect of emerging soil
540 cracks on runoff generation.

541

542 *VE1 Colpach Experiment 1, double gradient:* The reference representative hillslope (A1)
543 was selected to match the average hillslope length and elevation range of 241 delineated
544 hillslope profiles in the Colpach catchment (Figure 6 A). To check how strongly the
545 simulated stream flow depends on the gradient in relief energy we increased the elevation
546 range by a factor of two, yielding a maximum elevation of 108 m above the creek by a
547 preserved hillslope length.

548

549 *VE2 Colpach Experiment 2, bedrock topography:* To shed light on the role of bedrock
550 topography we compared four additional simulations with the reference model setup
551 (A1). In the second hillslope the 0.2 m thick bedrock interface was removed (VE2.1). In
552 the third hillslope we removed the bedrock-interface and assumed parallel bedrock
553 topography with the surface at 1 m depth (VE2.2). The fourth hillslope likewise has
554 surface bedrock topography at 1 m depth, but we added a no-flow boundary condition for
555 the lower 70 % of the right boundary to create a depression which has approximately the
556 same volume as all depressions in the reference slope (VE2.3). This approach is expected
557 to create a small storage volume that might create subsurface runoff by filling and
558 spilling, as shown by Graeff et al., (2009). Last not least, we used the reference hillslope
559 but removed the vertical macropores (VE2.4).

560

561 *VE3 Colpach Experiment 3, changed onset of phenological cycle:* The reference hillslope
562 employed a fixed phenological cycle for mixed forest, which was derived in the
563 Weiherbach catchment (Zehe et al., 2001). However, the start and end of the phenological
564 cycle is subject to inter-annual variations which can be described well by a temperature



565 index model proposed by Menzel et al., (2003). Hence, we changed the onset and end of
566 the vegetation period in the parameter table in accordance with the temperature index
567 model, while keeping unchanged the other temporal patterns in-between, like the leaf area
568 index or root depth.

569

570 *VE4 Wollefsbach Experiment 4, challenge of dealing with emergent soil structures:* The
571 fact that either worm burrows in spring/ fall or shrinkage cracks during dry spells in
572 midsummer control the soil hydraulic behavior and runoff formation in the Wollefsbach,
573 implies that the vertical flow paths in the model structure should be time-, or more
574 precisely, state-dependent. As CATFLOW does not treat soil hydraulic
575 parameters/macropores as state dependent but as constant, one cannot expect a rigid
576 parameter setup to reproduce the hydrographs in winter and summer in an acceptable
577 manner. This expectation was corroborated by our first simulation carried out with the
578 reference model for the Wollefsbach (A2). We hence tested the additional value of a state
579 dependent soil structure in a first tentative approach by subdividing the simulation period
580 into a winter and summer period, based on the temperature index model of Menzel et al.,
581 (2003). The winter period was simulated with the setup specified in the reference model
582 (A2) until the onset of the summer period. We then started a second simulation with an
583 elevated infiltrability using the final state of the first simulation as initial state.
584 Infiltrability was increased by an enlarged hydraulic conductivity of the upper 100 cm by
585 a factor of 25, 50 and 75 within three different model runs. Since the model run with the
586 factor 75 yielded the best results with respect to the discharge (estimated on KGE), we
587 used this model setup for the vegetation period in virtual experiment 4.

588 4. Results

589 4.1 Double mass curves and stream flow time series

590 As depicted in Figure 8 A and C the reference hillslope models A1 and A2 reproduced the
591 typical shape of the normalized double mass curves – the steep, almost linear increase in
592 the winter period and the transition to the much flatter summer regime – in both
593 catchments very well. This is further illustrated by the comparison of two typical
594 saturation patterns simulated for winter and summer in the Colpach (Figure 10 B). Local
595 bedrock depressions are close to saturation during the winter season, and hence ready to
596 create runoff by filling and spilling in response to rapid infiltration through vertical



597 macropores. These pools are, however, fairly dry during summer after a period of
598 transpiration and root water uptake. The absence of free water-sustaining fill and spill
599 runoff generation explains the flat summer regime in the double mass curves and thus the
600 dominant role of transpiration which may be sustained even by strongly bound soil water.
601 The KGEs of 0.87 and 0.94 in the Colpach and Wollefsbach corroborate that within the
602 error ranges both double mass curves are almost perfectly explained by the models. We
603 may hence state that the hillslope models closely portray the seasonal pattern of the
604 catchment's water balance, also because simulated and observed annual runoff
605 coefficients match very well (Table 2). A closer look at the simulated and observed runoff
606 time series (Figure 8 B and D) indicates, however, that the models performed differently
607 in both catchments in the winter and the summer season. Generally we observed in both
608 catchments a better matching of observed stream flow during the wet winter period and
609 clear deficiencies during dry summer conditions. For instance, the reference Colpach
610 model (A1) misses the steep and flashy runoff events in June and July (Figure 8 B). Note
611 that the representative hillslope model (A1) of the Colpach also performed well with
612 respect in matching the hydrograph of the previous year, with an NSE of 0.72.
613 Furthermore, the parameter setup was tested within uncalibrated simulations for the
614 Weierbach, a headwater in the same geological setting, again with acceptable results of a
615 KGE of 0.81 and a NSE of 0.68.

616 In the Wollefsbach we found visually even stronger seasonal differences in model
617 performance with respect to matching the hydrograph. This is further shown by the low
618 overall model performance of 0.26 for the NSE and 0.64 for the KGE in contrast to a
619 relative high logNSE of 0.82 (Table 2). The differences in the logNSE and NSE further
620 explain the strong influence of the overestimated runoff events in August and September
621 on the NSE that have almost no volume because of their short duration as a result of the
622 flashy runoff regime of the catchment. The reference model (A2) led to a strong
623 overestimation of runoff behavior in summer due to strong overland flow production
624 during convective events in August and September (Figure 8 D). No significant overland
625 flow was simulated during the rest of the year. This suggests that without the
626 representation of cracks by using separate summer macroporosity (VE4), soil infiltrability
627 is obviously too small compared to the real system as soon as cracks have emerged.



628 **4.2 Simulated and observed soil moisture dynamics**

629 It is of great interest as to what extent the model performance in reproducing soil
630 moisture or sap flow observations is consistent with the strengths and deficiencies of the
631 simulated hydrographs and double mass curves. Clearly we cannot expect that our
632 simulations are capable of reproducing the observed spatial variability of both distributed
633 data sources, as this needs a fully distributed model setup, which may have to account for
634 the variability of the terrestrial filter properties and of the rainfall and radiation forcing
635 within the catchment. A representative hillslope should, however, be ergodic and hence
636 match the averaged temporal dynamics and plot within the envelope of available soil
637 moisture observations, which are displayed in Figure 9 for both catchments and both
638 observation depths. Note that the spread in the observations in 10 cm is much larger in the
639 Colpach catchment, particularly in the dry months of June and July, while the opposite
640 holds true for soil moisture observations at 50 cm depth. This suggests that the
641 differences in runoff generation in the two catchments might also arise from differences
642 in storage and storage-related controls.

643

644 To estimate the representative soil moisture dynamics from the distributed observations
645 we employed a twelve-hour rolling median, which we compared to the spatially averaged
646 soil moisture simulated at the respective depths. Model goodness was determined visually
647 and by means of the KGE and the Spearman Rank correlation. Simulated soil moisture at
648 10 cm depth for the Colpach was systematically too high by around a volume of 25 %.
649 Yet the simulation is within the envelope that is spanned by the observations and the
650 KGE of 0.69 suggests some predictive power for top soil moisture. Also soil moisture
651 dynamics are matched well with a spearman rank correlation of 0.8. This holds true
652 especially if compared to the median of spearman rank correlations of all sensor pairs,
653 which is 0.66. In line with the findings presented in the previous section, the model
654 showed deficiencies in the summer period with respect to capturing the strong declines in
655 soil moisture in June and July. Simulated soil moisture at 50 cm exhibited a strong
656 positive bias as it is above the envelope spanned by the observations and has no
657 predictive power (KGE -0.89). Yet the changes in deeper soil moisture storage are in
658 good accordance, as reflected by the spearman rank correlation of 0.91.

659



660 Contrary to what we found in the Colpach, the simulation in 10 cm underestimated the
661 rolling median of soil moisture time series observed in the Wollefsbach (Figure 9 C); yet
662 it fell into the state space spanned by the observations. The predictive power is with a
663 KGE of 0.45 worse than in the Colpach, while the match of the temporal dynamics is,
664 with a rank correlation coefficient of 0.68, also slightly poorer. Again the model failed in
665 reproducing the strong decline in soil moisture between May and July. It is, however,
666 interesting to note that the model is nearly unbiased during August and September. This is
667 especially interesting since the reference model does not perform well with respect to the
668 discharge simulations in this time period. Simulated soil moisture at 50 cm depth showed
669 similar model deficiencies as found for the Colpach, while the bias was slightly smaller.

670 **4.3 Normalized simulated transpiration versus normalized sap flow velocities**

671 As sap flow provides a proxy for transpiration, we compared normalized, averaged sap
672 flow velocities of all beech and oak trees to the normalized simulated transpiration of the
673 reference hillslope model of the Colpach. Mean sap flow stayed close to zero until the end
674 of April and started to rise after the predicted onset of the vegetation period. In contrast,
675 simulated transpiration is already slightly above zero in January and exhibits a first peak
676 at the beginning of March. This indicates that the predefined phenological cycle is, as
677 expected, inappropriate for matching with the first sprout in this area. Simulations and
678 observations are in good accordance during midsummer. In the period between August
679 and October the simulations underestimate the observations, because the pre-defined
680 phenology declines too early. These deficiencies of the model to properly match onset
681 and end of the vegetation period are reflected in the rank correlation coefficient of 0.62.
682 Due to the fact that periods of high transpiration and sap flow activity have, while being
683 out of phase, a similar length, the model still matches the accumulated annual
684 evapotranspiration well and the annual water balance is reproduced properly.

685 **4.4 Virtual experiments to search for first-order controls**

686 *VE1 Colpach Experiment 1, double gradient:* Opposite to our expectation we found that
687 the doubling of the topographic gradient had only a minor effect on the simulated double
688 mass curves and hydrographs, respectively (Figure 11 F). The KGE decreased from 0.85
689 to 0.8 while logNSE increased from 0.75 to 0.85. In fact runoff peaks were slightly
690 smaller in the winter period compared to the reference hillslope model. While this appears



691 counterintuitive on first sight, it may be attributed to the decrease in subsurface storage
692 volumes in the bedrock depressions in the steeper hillslope.

693

694 *VE2 Colpach Experiment 2, bedrock topography:* Contrary to the VE1 this finding and in
695 line with our expectation, virtual experiment 2 revealed the key importance of bedrock
696 topography. The removal of the soil bedrock interface, which allowed for rapid flow in
697 the weathered schist, reduced the NSE to 0.8 and the KGE even more to 0.7 (Table 2),
698 mainly due to a reduction in simulated flood peaks (Figure 11 B). The key role of rapid
699 flow paths is further corroborated by the model run (VE 2.4) which left out the vertical
700 macropores from the reference setup (Figure 11 E); again simulated peaks are too small
701 and the KGE is reduced to 0.7. The removal of the bedrock depression by assuming
702 surface-parallel bedrock topography did completely change the simulated rainfall runoff
703 behavior (Figure 11 C). The corresponding hydrograph appears very much like a
704 separated base flow component due to the absence of peaks and high frequency
705 components; this is in line with the clear reduction of the NSE to 0.56 and the KGE to
706 0.59 (Table 2).

707

708 Most interestingly we found that the hillslope with the conceptualized depression in the
709 hill foot/riparian zone performed even marginally better than the reference setup,
710 particularly with the better match of the largest summer flood in August (Figure 11 D).
711 The corresponding KGE of 0.91 and NSE of 0.88 (Table 2) suggest a nearly perfect
712 performance within the error margins. We hence state that the results of virtual
713 experiment 2 are fully in line with our expectations for a system which works according
714 to the fill and spill concept. Yet, they provide a surprise, which is not so much the finding
715 that several bedrock architectures perform similarly well, but that the location and
716 connectedness of the bedrock seems to be of minor importance at this scale, as further
717 explained in the discussion.

718

719 *VE3 Colpach Experiment 3, changed onset of phenological cycle:* Our third virtual
720 experiment revealed that the improved representation of the onset and end of the
721 phenological cycle based on the temperature index model of Menzel et al., (2003) clearly
722 improved the model performance with respect to matching the observed onset of sap flow
723 activity (Figure 10 A). This went along with an improved simulation of the double mass
724 curves (Figure 12 A). Given a KGE of 0.95 and the fact that simulated and observed



725 annual runoff coefficients are with 0.54 and 0.56 in almost perfect accordance, this setup
726 is the most behavioral one of all tested setups (Table 2). A closer look at the simulated
727 hydrograph reveals also a clear improvement, particularly with respect to the logNSE
728 (Table 2). The more realistic runoff reaction in early summer can be explained by the fact
729 that bedrock depressions are still wet enough to create runoff due to the later onset of
730 transpiration. Yet the model still showed deficiencies, for instance, the overestimation of
731 the first runoff events in May and the underestimation of subsequent events in June and
732 July. The clear improvements which were already caused by this minor and
733 straightforward implementation of the dynamic onset of plant phenology suggests that
734 much more substantial improvements of transpiration controls might be a key for
735 substantially improving hydrological models.

736

737 *VE4 Wollefsbach Experiment 4, challenge of dealing with emergent soil structures:* The
738 virtual experiment in the Wollefsbach which uses a separated summer soil hydraulic
739 conductivity revealed and improved strongly matching runoff (Figure 8 D); this is
740 reflected in the increase in KGE from 0.64 to 0.76 and NSE from 0.26 to 0.74 compared
741 to the reference model (A2s). However the simple quick fix of multiplying the hydraulic
742 conductivity by 75 has also clear drawbacks, as the value was selected by manual
743 calibration on discharge. The model performance with respect to soil moisture became
744 clearly worse as shown in Figure 9 C and D. The overall spearman rank correlation
745 decrease to 0.51 at 10 cm depth, which can be explained by the fact that water flushes
746 through the soil at 10 and 50 cm to the bedrock interface due to the increased hydraulic
747 conductivity of the entire soil profile. We may hence state that such a quick fix of
748 increasing the hydraulic conductivity of the top soil to improve simulated stream flow
749 production is inappropriate for capturing the effect of emergent soil cracks for the right
750 reasons.

751 **5 Discussion**

752 This study provides strong evidence that physically based simulations with representative
753 hillslope models may closely portray water storage and release behavior of two distinctly
754 different lower mesoscale catchments. In line with the blueprint of Freeze and Harlan,
755 (1969) we disclaimed any form of calibration of the underlying model. Instead the model
756 structures were set up as one-to-one images of our perceptual models of the catchment



757 structure and the dominant processes, using a variety of different data and process
758 insights. Hillslope models were then parameterized according to the available very
759 diverse data as well as from the literature, within a handful of test simulations and
760 benchmarked against different response and storage measures without any additional
761 parameter tuning. In the following we discuss what can be learned from the successful
762 part of this approach with respect to a) the widely discussed role of soil heterogeneity and
763 preferential flow paths, b) the potential of physically based models to accommodate and
764 thus integrate multi-dimensional data, and c) the validity of the assumptions underlying
765 the representative hillslope concept. We then discuss the feasibility of the concept of
766 functional units and related to this, the partly astonishing findings we obtained within
767 three virtual experiments. Finally, we change perspective on the various deficiencies and
768 discuss the related inherent limitations of the representative hillslope concept itself and,
769 more importantly, the limitations of the theories underpinning physically based models,
770 with emphasis on bio-physical processes and emergent behavior. We conclude the
771 discussion with a final reflection on our notion of complexity and simplicity.

772 **5.1 Can a representative hillslope model mimic the functioning of a catchment?**

773 The attempt to model catchment behavior using a two-dimensional representative
774 hillslope implies a symmetry assumption in the sense that the water balance is dominated
775 by the interplay of hillslope parallel and vertical fluxes and the related driving gradients
776 (Zehe et al., 2014). This assumption is corroborated by the good but yet seasonally
777 dependent performance of both hillslope models with respect to matching the water
778 balance and the hydrographs. We particularly learn that the timing of runoff events in
779 these two catchments is controlled by the structural properties of the hillslopes,
780 particularly bedrock topography in concert with soil permeability. This is remarkable for
781 the Colpach catchment which has a size of 19.4 km², but in line with Robinson et al.,
782 (1995) who showed that catchments smaller than 20 km² are hillslope dominated. It is
783 obvious that a representative hillslope model cannot perform well as soon as the time
784 scales of flood routing and rainfall variability start dominating the response behavior and
785 timing of stream flow.

786

787 With respect to matching observed storage behavior both hillslope models had clear
788 deficiencies in simulating the observed average soil moisture data. While simulated and
789 observed average soil moisture dynamics were satisfyingly matched within the topsoil,



790 both models were biased at 50 cm depth. This might be explained by the fact that we used
791 a single soil type for the entire soil profile while porosity in the deeper ranges is most
792 likely lower (e.g. higher skeleton fraction). Particularly, the models failed in reproducing
793 the strong decline in soil moisture between May and July 2014. A likely reason for this is
794 that plant roots in the model extract water uniformly within the root zone, while plants
795 possibly optimize the amount of energy they have to invest to access soil water sustaining
796 transpiration (Hildebrandt et al., 2015). We also found that benchmarking of the model
797 against sap flow data provided additional information about the representation of
798 vegetation controls, which cannot be extracted from the double mass curve or discharge
799 data. We hence conclude that the proposed concept offers various opportunities for
800 integrating diverse field observations and testing their hydrological consistencies,
801 including soil water retention data and images from geophysics and dye staining
802 experiments. We further conclude that the idea of hillslope-scale functional units, which
803 act similarly with respect to runoff generation and might hence serve as building blocks
804 for catchment models, has been corroborated. This is particularly underpinned by the fact
805 that the parameterization of the reference model was – without tuning – transferable to a
806 headwater in the same geological setting. In this respect we were astonished by the fact
807 that the huge observed variability of soil water retention properties could be represented
808 in a rather straight forward manner.

809 **5.2 Is subsurface heterogeneity a dead end for a representative hillslope model?**

810 Both hillslopes were parametrized using a representative soil water retention curve using
811 experimental data from either 53 or 28 undisturbed soil cores within a maximum
812 likelihood approach. Since the two hillslope models are able to successfully simulate the
813 water balance, we may in line with Ebel and Loague, (2006) conclude that heterogeneity
814 of retention properties is not too important for reproducing runoff of lower mesoscale
815 catchments. This finding is also in line with the common knowledge that stream flow is a
816 low dimensional variable, which may be reproduced by a three to four parameter model.
817 We are fully aware that spatial variability of retention properties might be of importance
818 when dealing with solute transport or infiltration patterns in catchments. We also like to
819 stress that our approach may support the optimization of soil sampling with respect to the
820 minimum sample size that is needed to robustly determine a representative retention
821 curve for water balance modelling. We leave this here for further virtual experiments.

822



823 The fact that the overwhelming heterogeneity of subsurface must not be a dead end for
824 the idea of a representative hillslope model can also be concluded from our representation
825 of preferential flow. The straightforward implementation as connected flow paths
826 containing an artificial porous medium was sufficient to reproduce runoff generation and
827 the water balance for the whole time period in the Colpach and for the winter period in
828 the Wollefsbach catchment. This becomes more evident when looking at Figure 11 B and
829 F where the removal of either the bedrock interface or the vertical macropores reduced
830 the KGE from 0.84 to 0.72 and 0.71, respectively. Despite the known limitations of this
831 approach, or in fact of all approaches to simulate macropore flow (Beven and Germann,
832 2013), it seems that capturing the topology and connectedness of rapid flow paths is
833 crucial for setting up representative hillslopes at this scale. We also may conclude that
834 particularly the hydraulic properties of the macropores observed at other places
835 (Wienhöfer and Zehe, 2014; Klaus and Zehe, 2010) can be transferred across system
836 borders. But this fact should not be misinterpreted; it is not the exact position or the exact
837 extent of the macropore setup which is important but rather the hydraulic behavior of the
838 macropore medium and the idea of a connected flow path topology. We are aware that
839 such flow path topology is not uniquely defined, as shown by Wienhöfer and Zehe
840 (2014). It seems that equifinality and the concept of a representative hillslope is rather
841 more a blessing than a curse since there is an infinite number of possible macropore
842 setups which yield the same runoff characteristics. If this were not the case, we could not
843 transfer macropore setups from the literature across system borders and successfully
844 simulate two distinct runoff regimes which are strongly influenced by preferential flow.

845 **5.3 Hillslope scale structures as first order control on water storage and release**

846 **5.3.1 Is surface topography a first order control in the Colpach?**

847 The potential energy difference is a major control on runoff as runoff generation is mostly
848 driven by gravity. Nevertheless, surface topography can only be a poor means to
849 characterize relevant potential energy differences for runoff generation. For instance
850 Jackisch (2015) showed that variables extracted from topography could not explain
851 differences in runoff generation between the three geological settings of the Attert
852 catchment. Extracted topographic variables such as the topographic wetness index
853 suggested that two catchments, which produce runoff in a distinctly different fashion,
854 should operate similarly. Furthermore, Fenicia et al., (2016) report in the same research



855 area that a conceptual model built upon geological hydrological response units (HRU)
856 performed in a superior fashion with respect to explaining spatial variability of the
857 streamflow than a model built upon topographic HRUs. In line with this we found that a
858 doubled gradient in relief energy had almost no influence on the simulated water balance
859 in the Colpach, despite a marginal reduction of simulated flood peaks. The
860 counterintuitive peak reduction reflects the decrease in subsurface storage volume in the
861 bedrock depressions in the steeper hillslope. From this finding we may conclude that
862 runoff production in this highly permeable and highly porous soil setting is not limited by
863 the topographic gradient, as its doubling did not substantially increase subsurface flow
864 velocities. Nevertheless further virtual experiments with reduction of the topographic
865 gradient are needed to estimate the lower threshold above which simulations become
866 insensitive to gradient changes.

867 **5.3.2 Is bedrock topography a first order control in the Colpach?**

868 Contrary to the findings regarding surface topography our simulations were highly
869 sensitive to changes in bedrock topography and the presence/absence of a bedrock
870 interface and macropores. Particularly, the assumption of surface-parallel bedrock
871 changed the response behavior of the hillslope completely, by produced a hydrograph
872 which looked like a separated base flow component. Our findings fully corroborate the
873 argumentation of Wrede et al. (2015) who stated that the dominant runoff generation in
874 the Colpach works according to the fill and spill mechanism (Tromp-Van Meerveld and
875 McDonnell, 2006). In line with Hopp and McDonnell, (2009) we also found that local
876 depressions in bedrock topography and a varying soil depth jointly control filling and
877 spilling during subsurface runoff production. The real surprise of this virtual experiment
878 was, however, that the catchment scale fingerprint of a fill and spill system can be
879 simulated in several ways. One alternative was a spatially explicit representation of
880 bedrock topography as observed with electrical resistivity tomography at two typical
881 hillslopes, which implies that connectivity between these depressions depends on
882 subsurface wetness (Lehmann et al., 2006). The other feasible alternative was a hillslope
883 that combined surface-parallel bedrock topography with a large depression at the hill foot
884 sector, which had the same total storage volume as the explicit bedrock topography. This
885 second alternative produced a small riparian zone and performed even slightly better with
886 respect to matching the hydrograph. Hence we may conclude that it is not the detailed
887 representation of the subsurface architecture, including location of the depressions along



888 the slope line, but the correct representation of the total volume of all depressions which
889 makes up the behavioral catchment model. The last finding has important implications for
890 geophysical explorations of the shallow subsurface, as it is likely possible to extract a
891 representative catchment average storage volume from geophysical data at a few
892 hillslopes and translate this into a conceptualized storage volume in the model. This
893 procedure is most likely sufficient, which is promising as geophysical exploration of the
894 subsurface of each individual hillslope in a catchment is unfeasible.

895 **5.3.3 Is vegetation a first order control in the Colpach?**

896 The model performance with respect to matching the average sap flow dynamics and
897 particularly the results of the related virtual experiment 3 corroborates that the
898 phenological cycle of beech trees is a first order control on the water balance in this area.
899 As the onset of the vegetation phase depends strongly on the local climate setting, our
900 first simulation based on predefined phenological cycles was biased when the system
901 switched from dominance of abiotic controls to dominance of bio-physical controls. In
902 line with Seibert et al. (2016) we found that a simple temperature index proposed by
903 Menzel et al., (2003) is feasible for both detecting the tipping point between summer and
904 the winter regime in the double mass curve and to determine start and endpoint of the
905 vegetation phase in the model. This is underpinned by the model results with the
906 improved onset of the vegetation which showed indeed only small improvement in the
907 simulation of the discharge but an almost perfect fit of the normalized double mass curves
908 with a KGE of 0.95. As the SVAT modules need air temperature anyway, a dynamic
909 phenological cycle is straightforward to implement in CATFLOW.

910 **5.4 Limitations and challenges**

911 **5.4.1 The need to go distributed**

912 An example of the limitations of our single hillslope approach is the deficiencies that both
913 models encountered to capture flashy rainfall runoff events in the vegetation period.
914 Besides the existence of emergent structures, these events might likely be caused by
915 localized convective storms, probably with a strong contribution of the riparian zones
916 (Martínez-Carreras et al., 2015) and forest roads in the Colpach catchment and by
917 localized overland flow in the Wollefsbach catchment (Martínez-Carreras et al., 2012).
918 Such fingerprints of a non-uniform rainfall forcing cannot be captured by a simulation
919 with a single hillslope; it requires a distributed model setup and a river network.



920 Similarly, one cannot expect a single hillslope to reproduce the observed variability of
921 soil moisture and sap flow, which reflects the interplay of the spatial pattern in rainfall
922 and radiative forcing in combination with the heterogeneity of local soil and land use
923 properties. Yet we suggest that a representative hillslope model structure provides the
924 right start-up for a subsurface parameterization, i.e. a functional unit when setting up a
925 fully distributed catchment model consisting of several hillslopes and an interconnecting
926 river network. Simulations with distributed rainfall and using the same functional unit
927 parameterization for all hillslopes would tell how the variability in response and storage
928 behavior can be explained compared to the single hillslope. In the case where different
929 functional units are necessary to reproduce the variability of distributed fluxes and storage
930 dynamics, these can either be generated by further perturbation or one might choose to
931 measure the key variable in accordance with the virtual experiments. We also suggest that
932 our statistical approach to compare simulated and observed soil moisture and sap flow is
933 more appropriate than a point/grid cell-based evaluation. The latter technique would only
934 be appropriate in the case of perfect observations of rainfall and terrestrial properties with
935 perfect spatio-temporal resolution.

936 **5.4.2 The inherent limitations of the Richards equation**

937 The presented simulations are affected by inherent limitations of the Richards equation
938 and the approach we used to represent rapid flow. The major deficiency of the Richards
939 equation is the local equilibrium assumption and related to this, the assumption that
940 gravity driven flow and capillarity controlled flow are always controlled by the same
941 Darcian frictional loss term $k(\theta)$. This assumption can and should be relaxed particularly
942 during strong rainfall forcing, for instance by treating gravity flow as a separate advection
943 term. The related key challenges are not only the numerical solution of such an advection
944 diffusion equation but the proper representation of the energy loss for the advection and
945 the fact that kinetic energy of soil water flow may no longer be neglected. The limitations
946 of the Richards equation should not be mistaken for non-importance of capillary forces in
947 soils: there would be no soil water storage and probably no terrestrial vegetation without
948 capillary forces. Capillarity is a first-order control of soil water dynamics during radiation
949 driven conditions and the Darcy-Richards concept is sufficient for simulating soil water
950 dynamics in this context (Zehe et al., 2010, 2014).

951 Any physical theory or model, while being based on inference, is yet an empirical fit to
952 observables with its purpose to explain a class of phenomena as broadly as possible



953 (Popper, 1935). All physically-based models we use today are incomplete in the sense
954 that there are phenomena which fall outside their range of validity. A representative
955 hillslope model remains hence “a lousy model” as it needs to rely on an incomplete
956 description of the water fluxes in the catchment. Nevertheless, there is much to be learned
957 from imperfect solutions, as long as we are aware of their advantages and drawbacks and
958 as long as we stick to the blueprint of Freeze and Harlan (1969). Our study shows that
959 beside the usually discussed limitations, the real challenge is to deal with emergent
960 behavior. This is in fact a straightforward implication of the fact that both soil structure
961 and vegetation structure are rather “slowly” varying morphological state variables of the
962 hydrological system than constant/ stationary parameters. Soil structures in the clay-rich
963 soils of the Wollefsbach are non-stationary due to the active/ dormant phase of earth
964 worm burrows and due to crack formation during dry spells. Our use of summer and
965 winter macroporosity was a tentative first step to show the need and the potential of
966 treating hydraulic properties not as static but dynamic. A proper representation of such
967 non-linear feedbacks in physically based models is a two-fold challenge with respect to
968 gaining the necessary understanding of the underlying thresholds and with respect to
969 stability of the numerical solution when dealing with such a non-linear feedback.

970 **5.4.3 Bio-physical controls on transpiration –the weakest link in the chain?**

971 Numerical experiment 3 (VE3) corroborated that the improved representation of the onset
972 of the vegetation phase as a temperature dependent variable yielded superior simulations
973 of all forms of water release. While this was straightforward to implement, it remains a
974 tentative first step, because the evolution of plant morphological parameters remains the
975 same within every year. We argue that much more substantial improvements of bio-
976 physical controls might be the key for further improving the fundamental basis of our
977 models. The ideal solution is of course coupling with a dynamic vegetation model, as
978 proposed by Schymanski et al., (2008) or Tietjen et al., (2010) for pristine vegetation in
979 semi-arid areas. This implies that phenology evolves in response to climate and
980 hydrological controls, thereby creating feedbacks. It furthermore offers more realistic
981 ways for implementing root water uptake, as a distributed process along the root zone for
982 instance by optimizing the amount of energy plants have to invest to access soil water
983 (Hildebrandt et al., 2015). The challenge is, however, that ecological limitations in humid
984 regions are less obvious, which implies that these models cannot simply be transferred to
985 our regions. The coupling of hydrological models and crop models which have been



986 developed in an independent fashion is furthermore not a straightforward exercise
987 (Jackisch et al., 2014). Despite these challenges, we need a paradigm shift in accepting
988 that transpiration is part of the plant's metabolism, gas exchange and photosynthesis and
989 thus reflects (optimal) behavior of plants (Schymanski et al., 2009) rather than plants
990 acting as a water pump. The literature is full of different and much more realistic models
991 for parameterizing stomata conductance (Damour et al., 2010) that step beyond the heavy
992 parameterization of Jarvis (1972), which reflects the outworn paradigm of the “plant as
993 water pump”.

994 **6. Conclusions**

995 We overall conclude that perceptual models of catchments can be translated into
996 representative hillslope models which successfully portray the spatial aggregated
997 functioning. This was demonstrated for two distinctly different catchments and implies
998 that hillslope-scale functional units might indeed be identified as building blocks for
999 catchments and that their behavioral parameter sets are transferable within the same
1000 landscape setting. The general idea to translate a perceptual model into a model structure
1001 is not new and has already been applied with a conceptual rainfall-runoff model
1002 framework even within the same area (Wrede et al., 2015). Here the scientific asset is that
1003 we use a physically-based model which can be parameterized directly on field
1004 measurements since the parameters are directly related to the physical processes and their
1005 controlling structures. The drawback is that physically-based models are parameter
1006 intensive, limited due to the incomplete representation of physics and are data greedy
1007 which means that they need to be based on extensive field data which is only available in
1008 a few research catchments around the world. But what might seem like a drawback is also
1009 to their benefit since their simulations reflect naturally both the strength and limitations of
1010 the underlying representations of bio-physical processes. This offers the option to learn
1011 not only from the successful part of the study but particularly also from model
1012 deficiencies as they unmask limitations in the theoretical underpinnings and of the
1013 representative hillslope concept itself. We conclude that using physically-based models,
1014 even in such an aggregated and abstract manner provides insights into cause and effect
1015 relationships explaining what happens due to which reasons. This cannot be obtained to
1016 such an extent by conceptual models simply because they have been designed to
1017 reproduce rainfall-runoff relations as parsimoniously as possible. Their advantage is the



1018 simpler mathematical formulation and thereby a strong reduction in the number of
1019 parameters. This fact makes them easy to calibrate and hence the first choice for studies
1020 in data sparse catchments as well as for comparative hydrology. Nonetheless, a simple
1021 mathematical representation does not automatically mean that the model structures and
1022 the parameters are straightforward to interpret. This is evident not only in the fact that
1023 internal states and parameters of conceptual models are difficult to compare and derive
1024 from field observations, but also that their model structure is neither simple nor intuitive
1025 to interpret. As a consequence, model improvements and model comparisons often need
1026 to be benchmarked purely on a statistical foundation. Physically-based models are not
1027 based on simple mathematical equations, but their setup reflects much more intuitively
1028 the perception of the system, particularly in the subsurface.

1029 Therefore, we close with the note that simplicity in hydrology should not be mistaken for
1030 a mathematically simplified process description, parameter parsimony or minimum of
1031 model elements. To us it rather means achieving the perfect level of abstraction of the
1032 system we want to analyze – perfect in the sense of Antoine de Saint-Exupéry¹ –
1033 balancing necessary complexity with the greatest possible simplicity. A behavioral
1034 representative hillslope is hence not a simple average of all the existing hillslopes in a
1035 catchment but a behavioral, maybe not yet perfect, abstraction of a catchment – a picture
1036 in the sense of Heidegger.

1037

1038

¹ “A perfect picture is not achieved when there is nothing left to be added, but when there is nothing left to be taken away.” Antoine de Saint-Exupéry



1039 *Acknowledgements*

1040 This research contributes to the “Catchments As Organized Systems (CAOS)” research group (FOR 1598)
1041 funded by the German Science Foundation (DFG). Laurent Pfister and Jean-Francois Iffly from the
1042 Luxembourg Institute of Science and Technology (LIST) are acknowledged for organizing the permissions
1043 for the experiments and providing discharge data for Wollefsbach and Colpach. We furthermore thank the
1044 CAOS team of phase I, in particular subproject G, for providing soil moisture data as well as Malte Neuper
1045 for support, validation and discussions on the quality of the precipitation data.



1046 **References**

1047 Abrahamsen, P. and Hansen, S.: Daisy: an open soil-crop-atmosphere system model,
1048 Environ. Model. Softw., 15(3), 313–330, doi:10.1016/S1364-8152(00)00003-7, 2000.

1049 Bachmair, S. and Weiler, M.: Forest Hydrology and Biogeochemistry, edited by D. F.
1050 Levia, D. Carlyle-Moses, and T. Tanaka, Springer Netherlands, Dordrecht., 2011.

1051 Bárdossy, A.: Calibration of hydrological model parameters for ungauged catchments,
1052 Hydrol. Earth Syst. Sci. Discuss., 3(3), 1105–1124, doi:10.5194/hessd-3-1105-2006,
1053 2006.

1054 Bastardie, F., Capowiez, Y., De Dreuzy, J. R. and Cluzeau, D.: X-ray tomographic and
1055 hydraulic characterization of burrowing by three earthworm species in repacked soil
1056 cores, Appl. Soil Ecol., 24(1), 3–16, doi:10.1016/S0929-1393(03)00071-4, 2003.

1057 Beven, K.: Towards a coherent philosophy for modelling the environment, Proc. R. Soc.
1058 A Math. Phys. Eng. Sci., 458(2026), 2465–2484, doi:10.1098/rspa.2002.0986, 2002.

1059 Beven, K.: Streamflow Generation Processes: Introduction, 1st edition., edited by K. J.
1060 Beven, University of Lancaster, Lancaster, UK., 2006.

1061 Beven, K.: Rainfall-Runoff Modelling, second., John Wiley & Sons, Ltd, Chichester,
1062 UK., 2012.

1063 Beven, K. and Germann, P.: Macropores and water flow in soils revisited, Water Resour.
1064 Res., 49(6), 3071–3092, doi:10.1002/wrcr.20156, 2013.

1065 Bishop, J. M., Callaghan, M. V., Cey, E. E. and Bentley, L. R.: Measurement and
1066 simulation of subsurface tracer migration to tile drains in low permeability, macroporous
1067 soil, Water Resour. Res., 51(6), 3956–3981, doi:10.1002/2014WR016310, 2015.

1068 Bos, R. van den, Hoffmann, L., Juilleret, J., Matgen, P. and Pfister, L.: Conceptual
1069 modelling of individual HRU 's as a trade-off between bottom-up and top-down
1070 modelling , a case study ., in Conf. Environmental Modelling and Software. Proc. 3rd
1071 Biennial meeting of the international Environmental Modelling and Software Society.
1072 Vermont, USA., 1996.

1073 Bronstert, A. and Plate, E. J.: Modelling of runoff generation and soil moisture dynamics
1074 for hillslopes and micro-catchments, J. Hydrol., 198(1-4), 177–195, doi:10.1016/S0022-
1075 1694(96)03306-9, 1997.



- 1076 Burgess, S. S., Adams, M. a, Turner, N. C., Beverly, C. R., Ong, C. K., Khan, a a and
1077 Bleby, T. M.: An improved heat pulse method to measure low and reverse rates of sap
1078 flow in woody plants., *Tree Physiol.*, 21(9), 589–598, doi:10.1093/treephys/21.9.589,
1079 2001.
- 1080 Celia, M. A., Bouloutas, E. T. and Zarba, R. L.: A general mass-conservative numerical
1081 solution for the unsaturated flow equation, *Water Resour. Res.*, 26(7), 1483–1496,
1082 doi:10.1029/WR026i007p01483, 1990.
- 1083 Clark, M. P., Schaeffli, B., Schymanski, S. J., Samaniego, L., Luce, C. H., Jackson, B. M.,
1084 Freer, J. E., Arnold, J. R., Moore, R. D., Istanbuluoglu, E. and Ceola, S.: Improving the
1085 theoretical underpinnings of process-based hydrologic models, *Water Resour. Res.*, 52(3),
1086 2350–2365, doi:10.1002/2015WR017910, 2016.
- 1087 Damour, G., Simonneau, T., Cochard, H. and Urban, L.: An overview of models of
1088 stomatal conductance at the leaf level., *Plant. Cell Environ.*, 33(9), 1419–38,
1089 doi:10.1111/j.1365-3040.2010.02181.x, 2010.
- 1090 Dooge, J. C. I.: Looking for hydrologic laws, *Water Resour. Res.*, 22(9), 46S,
1091 doi:10.1029/WR022i09Sp0046S, 1986.
- 1092 Dunne, T. and Black, R. D.: Partial Area Contributions to Storm Runoff in a Small New
1093 England Watershed, *Water Resour. Res.*, 6(5), 1296–1311,
1094 doi:10.1029/WR006i005p01296, 1970.
- 1095 Ebel, B. a. and Loague, K.: Physics-based hydrologic-response simulation: Seeing
1096 through the fog of equifinality, *Hydrol. Process.*, 20(13), 2887–2900,
1097 doi:10.1002/hyp.6388, 2006.
- 1098 Ebel, B. a., Loague, K., Montgomery, D. R. and Dietrich, W. E.: Physics-based
1099 continuous simulation of long-term near-surface hydrologic response for the Coos Bay
1100 experimental catchment, *Water Resour. Res.*, 44(7), 1–23, doi:10.1029/2007WR006442,
1101 2008.
- 1102 Fenicia, F., Kavetski, D., Savenije, H. H. G., Clark, M. P., Schoups, G., Pfister, L. and
1103 Freer, J.: Catchment properties, function, and conceptual model representation: is there a
1104 correspondence?, *Hydrol. Process.*, 28(4), 2451–2467, doi:10.1002/hyp.9726, 2014.
- 1105 Fenicia, F., Kavetski, D., Savenije, H. H. G. and Pfister, L.: From spatially variable
1106 streamflow to distributed hydrological models: Analysis of key modeling decisions,
1107 *Water Resour. Res.*, (52), 1–36, doi:10.1002/2015WR017398, 2016.
- 1108 Freeze, R. A. and Harlan, R. L.: Blueprint for a physically-based, digitally-simulated



- 1109 hydrologic response model, *J. Hydrol.*, 9(3), 237–258, doi:10.1016/0022-1694(69)90020-
1110 1, 1969.
- 1111 Graeff, T., Zehe, E., Reusser, D., Lück, E., Schröder, B., Wenk, G., John, H. and
1112 Bronstert, A.: Process identification through rejection of model structures in a mid-
1113 mountainous rural catchment: observations of rainfall-runoff response, geophysical
1114 conditions and model inter-comparison, *Hydrol. Process.*, 23(5), 702–718,
1115 doi:10.1002/hyp.7171, 2009.
- 1116 Grayson, R. B., Moore, I. D. and McMahon, T. A.: Physically based hydrologic
1117 modeling: 2. Is the concept realistic?, *Water Resour. Res.*, 28(10), 2659–2666,
1118 doi:10.1029/92WR01259, 1992.
- 1119 Gupta, H. V., Kling, H., Yilmaz, K. K. and Martinez, G. F.: Decomposition of the mean
1120 squared error and NSE performance criteria: Implications for improving hydrological
1121 modelling, *J. Hydrol.*, 377(1-2), 80–91, doi:10.1016/j.jhydrol.2009.08.003, 2009.
- 1122 Gupta, H. V., Clark, M. P., Vrugt, J. a., Abramowitz, G. and Ye, M.: Towards a
1123 comprehensive assessment of model structural adequacy, *Water Resour. Res.*, 48(8), 1–
1124 16, doi:10.1029/2011WR011044, 2012.
- 1125 Hassanizadeh, S. M., Celia, M. A. and Dahle, H. K.: Dynamic effect in the capillary
1126 pressure–saturation relationship and its impacts on unsaturated flow, *Vadose Zo. J.*, 1,
1127 38–57, 2002.
- 1128 Haws, N., Rao, P., Simunek, J. and Poyer, I.: Single-porosity and dual-porosity modeling
1129 of water flow and solute transport in subsurface-drained fields using effective field-scale
1130 parameters, *J. Hydrol.*, 2005.
- 1131 Heidegger, M.: The age of the world picture, *Quest. Concern. Technol. other essays*,
1132 1977.
- 1133 Hildebrandt, A., Kleidon, A. and Bechmann, M.: A thermodynamic formulation of root
1134 water uptake, *Hydrol. Earth Syst. Sci. Discuss.*, 12(12), 13383–13413, doi:10.5194/hessd-
1135 12-13383-2015, 2015.
- 1136 Hopp, L. and McDonnell, J. J.: Connectivity at the hillslope scale: Identifying interactions
1137 between storm size, bedrock permeability, slope angle and soil depth, *J. Hydrol.*, 376(3-
1138 4), 378–391, doi:10.1016/j.jhydrol.2009.07.047, 2009.
- 1139 Jackisch, C.: Linking structure and functioning of hydrological systems., KIT -
1140 Karlsruher Institut of Technology., 2015.



- 1141 Jackisch, C., Zehe, E., Samaniego, L. and Singh, A. K.: An experiment to gauge an
1142 ungauged catchment: rapid data assessment and eco-hydrological modelling in a data-
1143 scarce rural catchment, *Hydrol. Sci. J.*, 59(12), 2103–2125,
1144 doi:10.1080/02626667.2013.870662, 2014.
- 1145 Jarvis, P. G.: The Interpretation of the Variations in Leaf Water Potential and Stomatal
1146 Conductance Found in Canopies in the Field, *Philos. Trans. R. Soc. B Biol. Sci.*,
1147 273(927), 593–610, doi:10.1098/rstb.1976.0035, 1976.
- 1148 Juilleret, J., Iffly, J. F., Pfister, L. and Hissler, C.: Remarkable Pleistocene periglacial
1149 slope deposits in Luxembourg (Oesling): pedological implication and geosite potential,
1150 *Bull. la Société des Nat. Luxemb.*, 112(1), 125–130, 2011.
- 1151 Katuwal, S., Moldrup, P., Lamandé, M., Tuller, M. and de Jonge, L. W.: Effects of CT
1152 Number Derived Matrix Density on Preferential Flow and Transport in a Macroporous
1153 Agricultural Soil, *Vadose Zo. J.*, 14(7), 0, doi:10.2136/vzj2015.01.0002, 2015.
- 1154 Kirchner, J. W.: Getting the right answers for the right reasons: Linking measurements,
1155 analyses, and models to advance the science of hydrology, *Water Resour. Res.*, 42(3),
1156 doi:10.1029/2005WR004362, 2006.
- 1157 Kirkby, M.: Tests of the random network model, and its application to basin hydrology,
1158 *Earth Surf. Process.*, 1(August 1975), 197–212, doi:10.1002/esp.3290010302, 1976.
- 1159 Klaus, J. and Zehe, E.: Modelling rapid flow response of a tile-drained field site using a
1160 2D physically based model: assessment of “equifinal” model setups, *Hydrol. Process.*,
1161 24(12), 1595–1609, doi:10.1002/hyp.7687, 2010.
- 1162 Klaus, J. and Zehe, E.: A novel explicit approach to model bromide and pesticide
1163 transport in connected soil structures, *Hydrol. Earth Syst. Sci.*, 15(7), 2127–2144,
1164 doi:10.5194/hess-15-2127-2011, 2011.
- 1165 Köhne, J. M., Mohanty, B. P. and Šimůnek, J.: Inverse Dual-Permeability Modeling of
1166 Preferential Water Flow in a Soil Column and Implications for Field-Scale Solute
1167 Transport, *Vadose Zo. J.*, 5(1), 59, doi:10.2136/vzj2005.0008, 2006.
- 1168 Kucharik, C. J. and Brye, K. R.: Integrated BIOSphere Simulator (IBIS) Yield and Nitrate
1169 Loss Predictions for Wisconsin Maize Receiving Varied Amounts of Nitrogen Fertilizer,
1170 *J. Environ. Qual.*, 32(1), 247, doi:10.2134/jeq2003.2470, 2003.
- 1171 Lehmann, P., Hinz, C., McGrath, G., Tromp-van Meerveld, H.-J. and McDonnell, J. J.:
1172 Rainfall threshold for hillslope outflow: an emergent property of flow pathway
1173 connectivity, *Hydrol. Earth Syst. Sci. Discuss.*, 3(5), 2923–2961, doi:10.5194/hessd-3-



1174 2923-2006, 2006.

1175 Loague, K. and VanderKwaak, J. E.: Physics-based hydrologic response simulation:
1176 Platinum bridge, 1958 Edsel, or useful tool, *Hydrol. Process.*, 18(15), 2949–2956,
1177 doi:10.1002/hyp.5737, 2004.

1178 Loke, M.: Rapid 2D Resistivity & IP Inversion using the least-squares method, *Geotomo*
1179 *Software, Man.*, 2003.

1180 Martínez-Carreras, N., Krein, A., Gallart, F., Iffly, J.-F., Hissler, C., Pfister, L.,
1181 Hoffmann, L. and Owens, P. N.: The Influence of Sediment Sources and Hydrologic
1182 Events on the Nutrient and Metal Content of Fine-Grained Sediments (Attert River Basin,
1183 Luxembourg), *Water, Air, Soil Pollut.*, 223(9), 5685–5705, doi:10.1007/s11270-012-
1184 1307-1, 2012.

1185 Martínez-Carreras, N., Wetzel, C. E., Frentress, J., Ector, L., McDonnell, J. J., Hoffmann,
1186 L. and Pfister, L.: Hydrological connectivity inferred from diatom transport through the
1187 riparian-stream system, *Hydrol. Earth Syst. Sci.*, 19(7), 3133–3151, doi:10.5194/hess-19-
1188 3133-2015, 2015.

1189 Maurer, T.: Physikalisch begründete zeitkontinuierliche Modellierung des
1190 Wassertransports in kleinen ländlichen Einzugsgebieten., *Karlsruher Institut für*
1191 *Technologie.*, 1997.

1192 Menzel, A., Jakobi, G., Ahas, R., Scheifinger, H. and Estrella, N.: Variations of the
1193 climatological growing season (1951-2000) in Germany compared with other countries,
1194 *Int. J. Climatol.*, 23(7), 793–812, doi:10.1002/joc.915, 2003.

1195 Mueller, E. N., Güntner, A., Francke, T. and Mamede, G.: Modelling sediment export,
1196 retention and reservoir sedimentation in drylands with the WASA-SED model, *Geosci.*
1197 *Model Dev.*, 3(1), 275–291, doi:10.5194/gmd-3-275-2010, 2010.

1198 Or, D.: Scaling of capillary, gravity and viscous forces affecting flow morphology in
1199 unsaturated porous media, *Adv. Water Resour.*, 31(9), 1129–1136,
1200 doi:10.1016/j.advwatres.2007.10.004, 2008.

1201 Or, D., Lehmann, P. and Assouline, S.: Natural length scales define the range of
1202 applicability of the Richards equation for capillary flows, *Water Resour. Res.*, 51(9),
1203 7130–7144, doi:10.1002/2015WR017034, 2015.

1204 Peters, A. and Durner, W.: Simplified evaporation method for determining soil hydraulic
1205 properties, *J. Hydrol.*, 356(1-2), 147–162, doi:10.1016/j.jhydrol.2008.04.016, 2008.



1206 Pfister, L., Humbert, J. and Hoffmann, L.: Recent trends in rainfall-runoff characteristics
1207 in the Alzette River basin, Luxembourg, *Clim. Change*, 45(1996), 323–337,
1208 doi:10.1023/A:1005567808533, 2000.

1209 Popper, K.: *Logik der Forschung*, First engl., Verlag von Julius Springer, Vienna,
1210 Austria., 1935.

1211 Robinson, J. S., Sivapalan, M. and Snell, J. D.: On the relative roles of hillslope
1212 processes, channel routing, and network geomorphology in the hydrologic response of
1213 natural catchments, *Water Resour. Res.*, 31(12), 3089–3101, doi:10.1029/95WR01948,
1214 1995.

1215 Rodriguez-Iturbe, I., D’Odorico, P., Porporato, A. and Ridolfi, L.: On the spatial and
1216 temporal links between vegetation, climate, and soil moisture, *Water Resour. Res.*,
1217 35(12), 3709–3722, doi:10.1029/1999WR900255, 1999.

1218 Sander, T. and Gerke, H. H.: Modelling field-data of preferential flow in paddy soil
1219 induced by earthworm burrows, *J. Contam. Hydrol.*, 104(1-4), 126–136,
1220 doi:10.1016/j.jconhyd.2008.11.003, 2009.

1221 Schymanski, S. J., Sivapalan, M., Roderick, M. L., Beringer, J. and Hutley, L. B.: An
1222 optimality-based model of the coupled soil moisture and root dynamics, *Hydrol. Earth
1223 Syst. Sci.*, 12(3), 913–932, doi:10.5194/hessd-5-51-2008, 2008.

1224 Schymanski, S. J., Sivapalan, M., Roderick, M. L., Hutley, L. B. and Beringer, J.: An
1225 optimality-based model of the dynamic feedbacks between natural vegetation and the
1226 water balance, *Water Resour. Res.*, 45(1), doi:10.1029/2008WR006841, 2009.

1227 Seibert, J. and McDonnell, J. J.: On the dialog between experimentalist and modeler in
1228 catchment hydrology: Use of soft data for multicriteria model calibration, *Water Resour.
1229 Res.*, 38(11), 23–1–23–14, doi:10.1029/2001WR000978, 2002.

1230 Seibert, S. P., Jackisch, C., Ehret, U., Pfister, L. and Zehe, E.: Exploring the interplay
1231 between state, structure and runoff behaviour of lower mesoscale catchments, *Hydrol.
1232 Earth Syst. Sci. Discuss.*, 1–51, doi:10.5194/hess-2016-109, 2016.

1233 Shipitalo, M. and Butt, K.: Occupancy and geometrical properties of *Lumbricus terrestris*
1234 L. burrows affecting infiltration, *Pedobiologia (Jena)*, 43, 782–794, 1999.

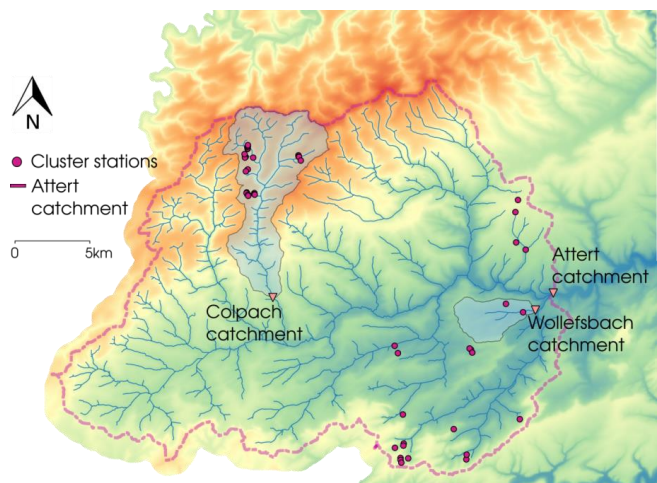
1235 Simmons, C. S.: A stochastic-convective transport representation of dispersion in one-
1236 dimensional porous media systems, *Water Resour. Res.*, 18(4), 1193–1214,
1237 doi:10.1029/WR018i004p01193, 1982.



- 1238 Simunek, J., Jarvis, N. J., van Genuchten, M. T. and Gardenas, A.: Review and
1239 comparison of models for describing non-equilibrium and preferential flow and transport
1240 in the vadose zone, *J. Hydrol.*, 272, 14–35, doi:10.1016/S0022-1694(02)00252-4, 2003.
- 1241 Tietjen, B. and Jeltsch, F.: Semi-arid grazing systems and climate change: a survey of
1242 present modelling potential and future needs, *J. Appl. Ecol.*, 44(2), 425–434,
1243 doi:10.1111/j.1365-2664.2007.01280.x, 2007.
- 1244 Tietjen, B., Jeltsch, F., Zehe, E., Classen, N., Groengroeft, A., Schiffers, K. and Oldeland,
1245 J.: Effects of climate change on the coupled dynamics of water and vegetation in
1246 drylands, *Ecohydrology*, 3, 226–237, doi:10.1002/eco.70, 2010.
- 1247 Tromp-Van Meerveld, H. J. and McDonnell, J. J.: Threshold relations in subsurface
1248 stormflow: 2. The fill and spill hypothesis, *Water Resour. Res.*, 42(August 2005), 1–11,
1249 doi:10.1029/2004WR003800, 2006.
- 1250 Vogel, H. J. and Roth, K.: Quantitative morphology and network representation of soil
1251 pore structure, *Adv. Water Resour.*, 24(3-4), 233–242, doi:10.1016/S0309-
1252 1708(00)00055-5, 2001.
- 1253 Weiler, M. and McDonnell, J.: Virtual experiments: a new approach for improving
1254 process conceptualization in hillslope hydrology, *J. Hydrol.*, 285(1-4), 3–18,
1255 doi:10.1016/S0022-1694(03)00271-3, 2004.
- 1256 Wienhöfer, J. and Zehe, E.: Predicting subsurface stormflow response of a forested
1257 hillslope – the role of connected flow paths, *Hydrol. Earth Syst. Sci.*, 18(1), 121–138,
1258 doi:10.5194/hess-18-121-2014, 2014.
- 1259 Wrede, S., Fenicia, F., Martínez-Carreras, N., Juilleret, J., Hissler, C., Krein, A., Savenije,
1260 H. H. G., Uhlenbrook, S., Kavetski, D. and Pfister, L.: Towards more systematic
1261 perceptual model development: a case study using 3 Luxembourgish catchments, *Hydrol.*
1262 *Process.*, 29(12), 2731–2750, doi:10.1002/hyp.10393, 2015.
- 1263 Zehe, E. and Blöschl, G.: Predictability of hydrologic response at the plot and catchment
1264 scales: Role of initial conditions, *Water Resour. Res.*, 40(10), 1–21,
1265 doi:10.1029/2003WR002869, 2004.
- 1266 Zehe, E., Maurer, T., Ihringer, J. and Plate, E.: Modeling water flow and mass transport in
1267 a loess catchment, *Phys. Chem. Earth, Part B Hydrol. Ocean. Atmos.*, 26(7-8), 487–507,
1268 doi:10.1016/S1464-1909(01)00041-7, 2001.
- 1269 Zehe, E., Becker, R., Bárdossy, A. and Plate, E.: Uncertainty of simulated catchment
1270 runoff response in the presence of threshold processes: Role of initial soil moisture and



- 1271 precipitation, *J. Hydrol.*, 315(1-4), 183–202, doi:10.1016/j.jhydrol.2005.03.038, 2005.
- 1272 Zehe, E., Lee, H., Sivapalan, M. and Dynamical, M. S.: Dynamical process upscaling for
1273 deriving catchment scale state variables and constitutive relations for meso-scale process
1274 models To cite this version : Dynamical process upscaling for deriving catchment scale
1275 state variables and constitutive relations fo, 2006.
- 1276 Zehe, E., Elsenbeer, H., Lindenmaier, F., Schulz, K. and Blöschl, G.: Patterns of
1277 predictability in hydrological threshold systems, *Water Resour. Res.*, 43(7),
1278 doi:10.1029/2006WR005589, 2007.
- 1279 Zehe, E., Graeff, T., Morgner, M., Bauer, A. and Bronstert, A.: Plot and field scale soil
1280 moisture dynamics and subsurface wetness control on runoff generation in a headwater in
1281 the Ore Mountains, *Hydrol. Earth Syst. Sci.*, 14(6), 873–889, doi:10.5194/hess-14-873-
1282 2010, 2010a.
- 1283 Zehe, E., Blume, T. and Blöschl, G.: The principle of “maximum energy dissipation”: a
1284 novel thermodynamic perspective on rapid water flow in connected soil structures, *Philos.*
1285 *Trans. R. Soc. London B Biol. Sci.*, 365(1545), 1377–1386, doi:10.1098/rstb.2009.0308,
1286 2010b.
- 1287 Zehe, E., Ehret, U., Blume, T., Kleidon, a., Scherer, U. and Westhoff, M.: A
1288 thermodynamic approach to link self-organization, preferential flow and rainfall–runoff
1289 behaviour, *Hydrol. Earth Syst. Sci.*, 17(11), 4297–4322, doi:10.5194/hess-17-4297-2013,
1290 2013.
- 1291 Zehe, E., Ehret, U., Pfister, L., Blume, T., Schröder, B., Westhoff, M., Jackisch, C.,
1292 Schymanski, S. J., Weiler, M., Schulz, K., Allroggen, N., Tronicke, J., Dietrich, P.,
1293 Scherer, U., Eccard, J., Wulfmeyer, V. and Kleidon, A.: HESS Opinions: Functional
1294 units: a novel framework to explore the link between spatial organization and
1295 hydrological functioning of intermediate scale catchments, *Hydrol. Earth Syst. Sci.*
1296 *Discuss.*, 11(3), 3249–3313, doi:10.5194/hessd-11-3249-2014, 2014.
- 1297



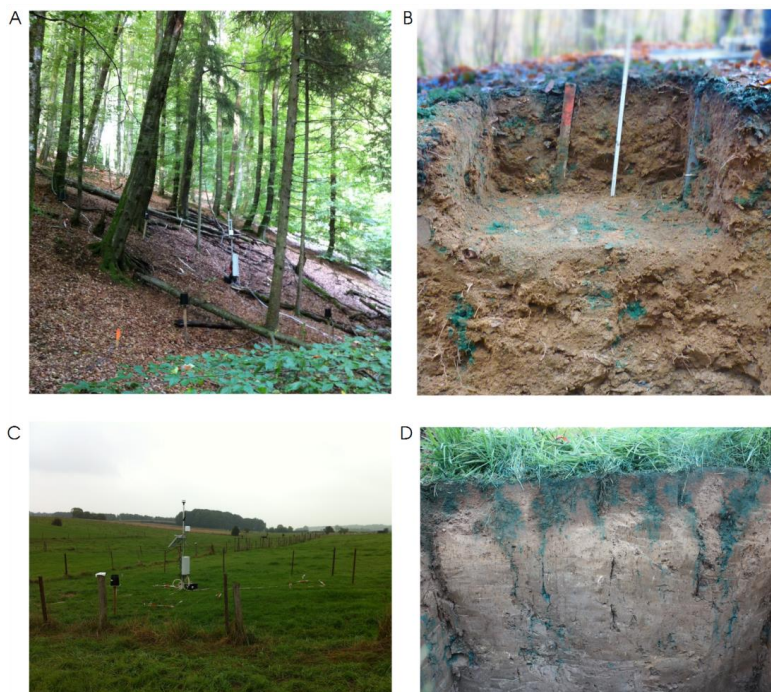
1298

1299 **Figure 1** Map of the Atert basin with the two selected headwater catchments of this study (Colpach and
1300 **Wollefsbach**). In addition, the cluster sites of the CAOS research unit are displayed.

1301



1302

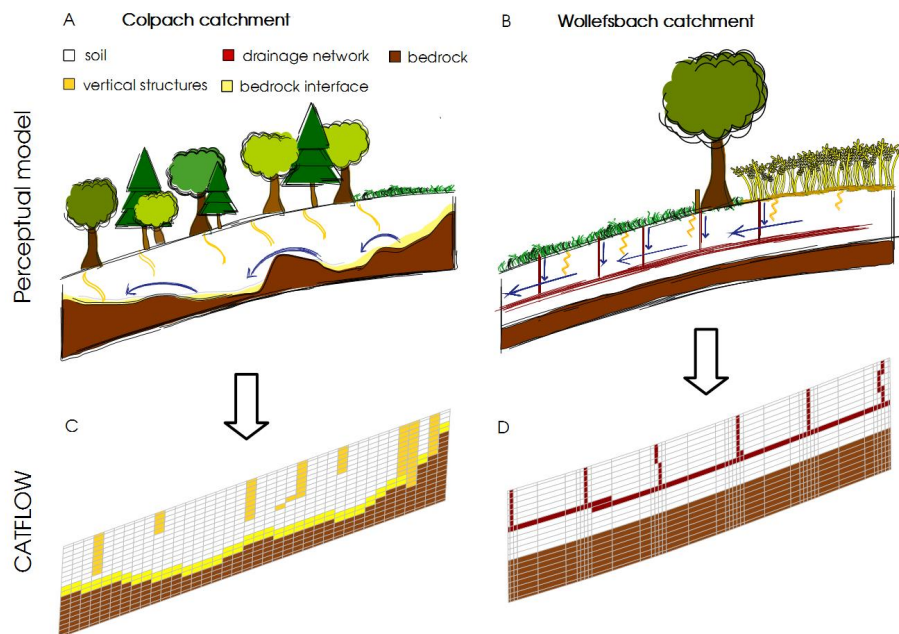


1303

1304 Figure 2 (A) Typical steep forested hillslope in the Colpach catchment; (B) Soil profile in the Colpach catchment
1305 after a brilliant blue sprinkling experiment was conducted. The punctual appearance of blue color illustrates the
1306 influence of vertical structures on soil water movement in this Schist area. (C) Plain pasture site of the
1307 Wollefsbach catchment; (D) Soil profile in the Wollefsbach catchment after a brilliant blue experiment showing
1308 the influence of soil cracks and vertical structures on the soil water movement.

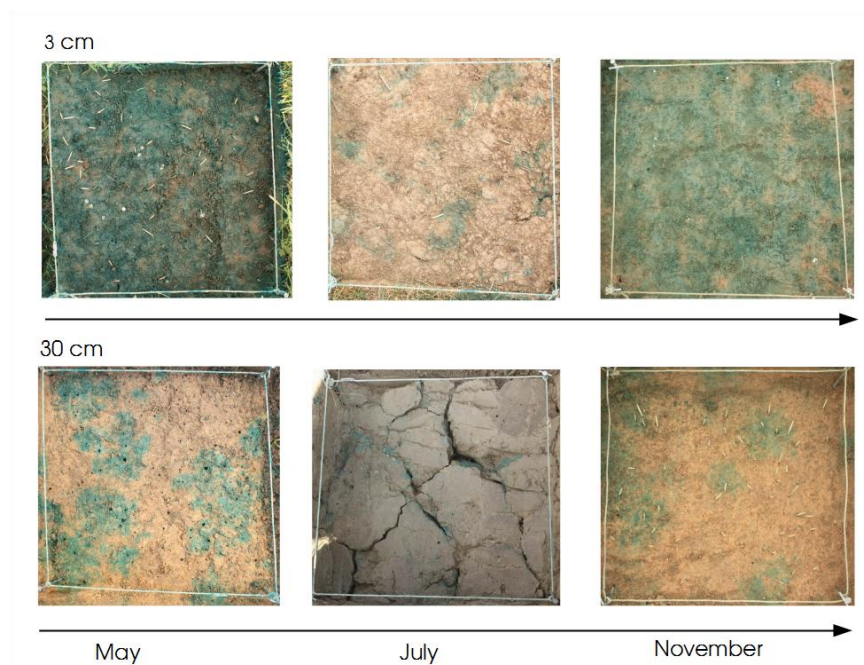


1309



1310

1311 **Figure 3** Perceptual models of the (A) Colpach and (B) Wollefsbach and their translation into a representative
1312 hillslope model for CATFLOW. Small sections of the CATFLOW hillslope are displayed for the (C) Colpach and
1313 for the (D) Wollefsbach.



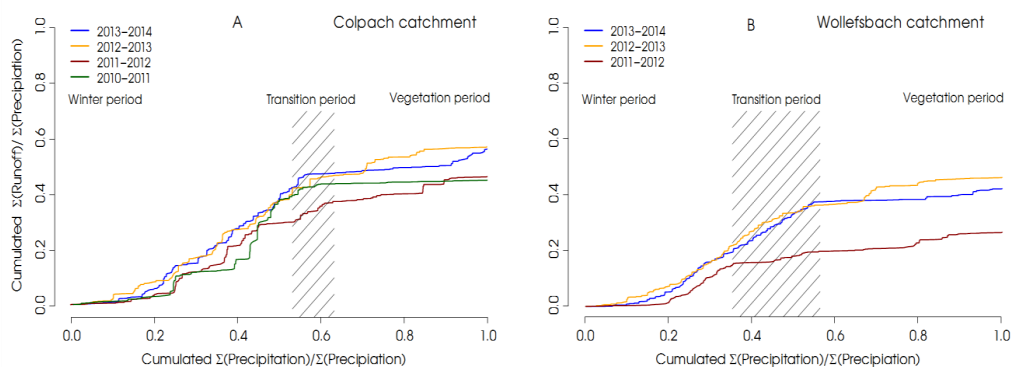
1314

1315 **Figure 4 Emergent structures in the Wollefsbach catchment for the sampling dates. In May macropore flow**
1316 **through earth worm burrows dominates infiltration, while in July clearly visible soil cracks occur. In contrast, a**
1317 **more homogenous infiltration pattern is visible in November, especially at 3 cm depth.**

1318



1319



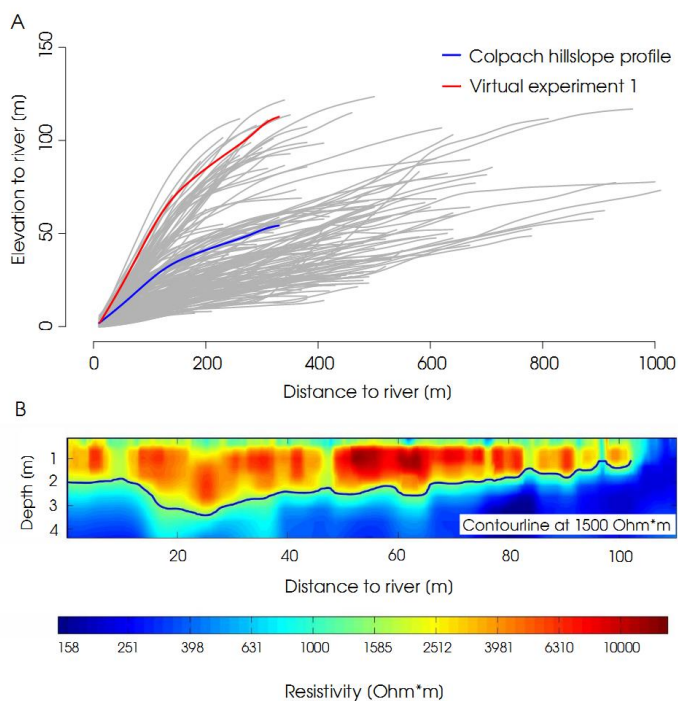
1320

1321 **Figure 5** Normalized double mass curves for each hydrological year from 2010 to 2014 in the Colpach catchment
1322 (A) and from 2011 to 2014 in the Wollefsbach catchment (B). The transition period marks the time of the years
1323 when the catchment shifts from the winter period to the vegetation period. The separation of the seasons is based
1324 on a temperature index model from Menzel et al., (2003). Since the season shift varies between the hydrological
1325 years the transition period is displayed as an area.

1326



1327



1328

1329 **Figure 6 (A) Profile of all hillslope extracted from a DEM in the Colpach catchment. The two hillslope profiles**
1330 **we used in this study are highlighted in blue (reference model setup) and red (virtual experiment 1 (VE1) steeper**
1331 **hillslope). (B) Bedrock topography of a hillslope in the Schist area measured using ERT. The contour line**
1332 **displays the 1500 Ω m isoline which is interpreted as soil bedrock interface.**

1333

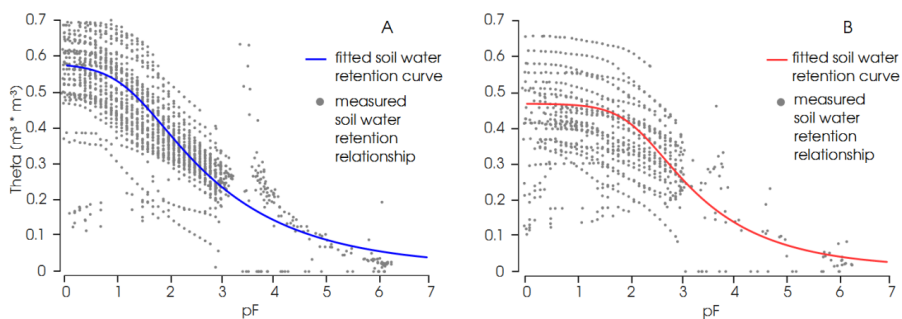
1334

1335

1336

1337

1338



1339

1340 **Figure 7 Fitted soil water retention curves and measured soil water retention relationships for the Colpach (A)**
1341 **and Wollefsbach (B) catchment.**

1342

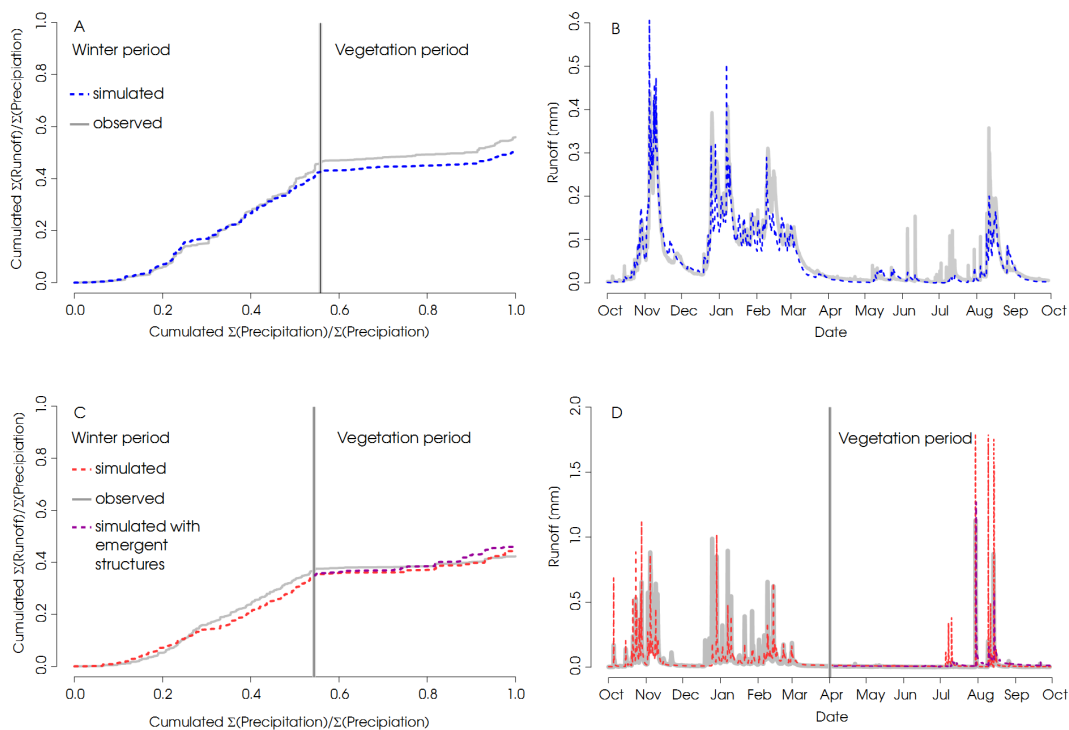


1343 **Table 1 Hydraulic and transport parameter values used for different materials in the basic model setups.**

Type of structure	Saturated hydraulic conductivity K_s ($m\ s^{-1}$)	Total porosity Θ_s (-)	Residual water content Θ_r (-)	Reciprocal entry value α (m^{-1})	air Shape parameter n (-)
<i>Colpach</i>					
Soil layer	5×10^{-4}	0.57	0.05	6.45	1.5
Soil bedrock interface	2×10^{-3}	0.35	0.05	7.5	1.5
Bedrock	1×10^{-9}	0.4	0.05	0.5	2
<i>Wollefsbach</i>					
Soil layer	2.92×10^{-4}	0.46	0.05	0.66	1.1
Drainage system	2×10^{-3}	0.25	0.1	7.5	1.5
Bedrock	5×10^{-9}	0.45	0.11	0.5	2

1344

1345



1346

1347 **Figure 8** Simulated and observed normalized double mass curves of the Colpach (A) and the Wollefsbach (C)
 1348 catchment. The double mass curves are separated into a winter and a vegetation period after Menzel et al.,
 1349 (2003). The simulated runoff against the observed runoff are displayed in (B) for the Colpach and in (D) for the
 1350 Wollefsbach. Moreover, in (D) the simulation period is separated into a winter and vegetation period and the
 1351 model result with the emergent structures through the increased hydraulic conductivity (VE4) is displayed for
 1352 the vegetation period.

1353



1354

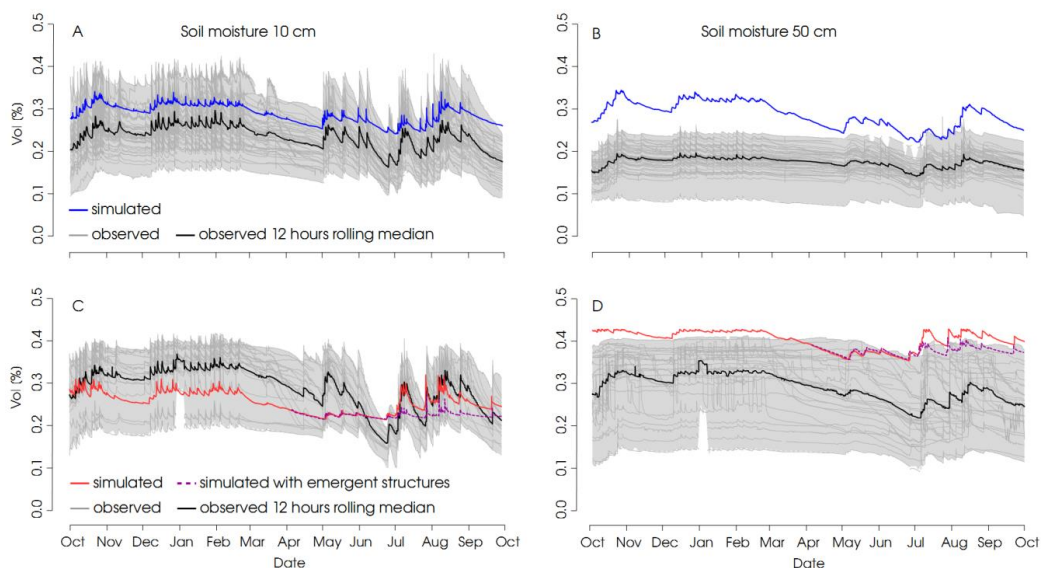
1355 **Table 2 Benchmarks for simulated double mass curves and simulated discharge for all model setups used in this**
 1356 **study.**

Model setup	<i>Double mass curve:</i>		<i>Discharge:</i>	
	KGE	NSE	LogNSE	KGE
<i>Colpach models</i>				
A1: Reference Colpach model	0.87	0.84	0.75	0.85
<i>Virtual Experiments 1</i>				
VE1: Steeper topography	0.86	0.81	0.85	0.8
<i>Virtual Experiments 2</i>				
VE2.1: No bedrock interface	0.82	0.8	0.72	0.72
VE2.2: Parallel bedrock	0.78	0.56	0.69	0.59
VE2.3: Conceptualized storage	0.95	0.88	0.8	0.91
VE2.4: No vertical structures	0.71			
<i>Virtual Experiments 3</i>				
VE3: Improved starting point for the phenological cycle	0.95	0.84	0.8	0.86
<i>Wollefsbach models</i>				
A2: Reference Wollefsbach model	0.94	0.26	0.82	0.64
<i>Virtual Experiment 4</i>				
VE4: Emergent structures	0.95	0.74	0.61	0.76

1357

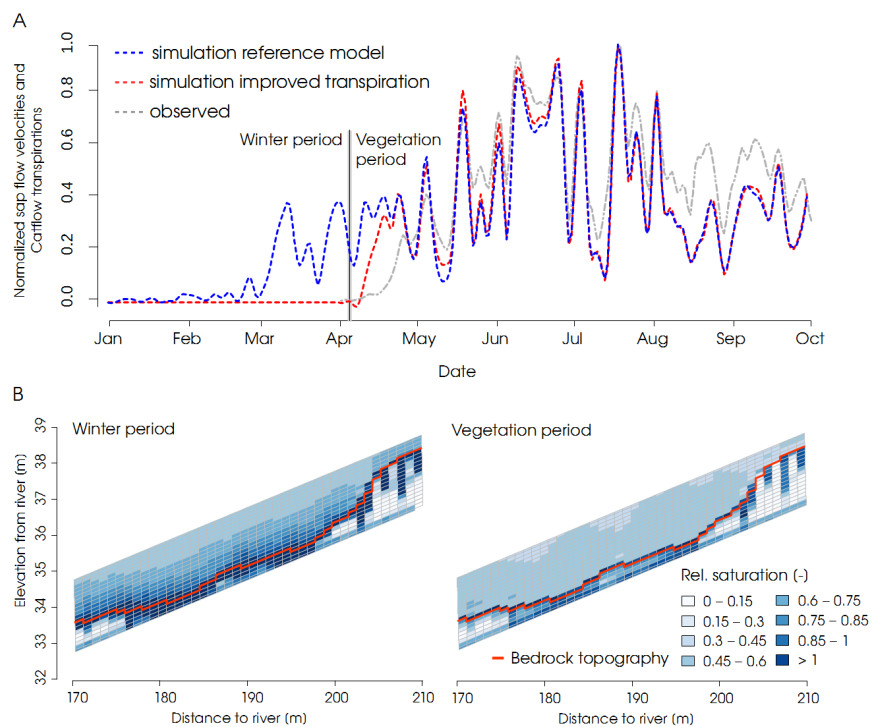


1358



1359

1360 **Figure 9** Observed soil moisture at 10 and 50 cm depths in the schist (A and B) and marl (C and D) area of the
1361 **Attert** catchment. Additionally the 12 hours rolling median (black) derived from the soil moisture observations
1362 and the simulated soil moisture dynamics at the respective depths (blue Colpach; red Wollefsbach; green
1363 Wollefsbach with emergent structures) are displayed.

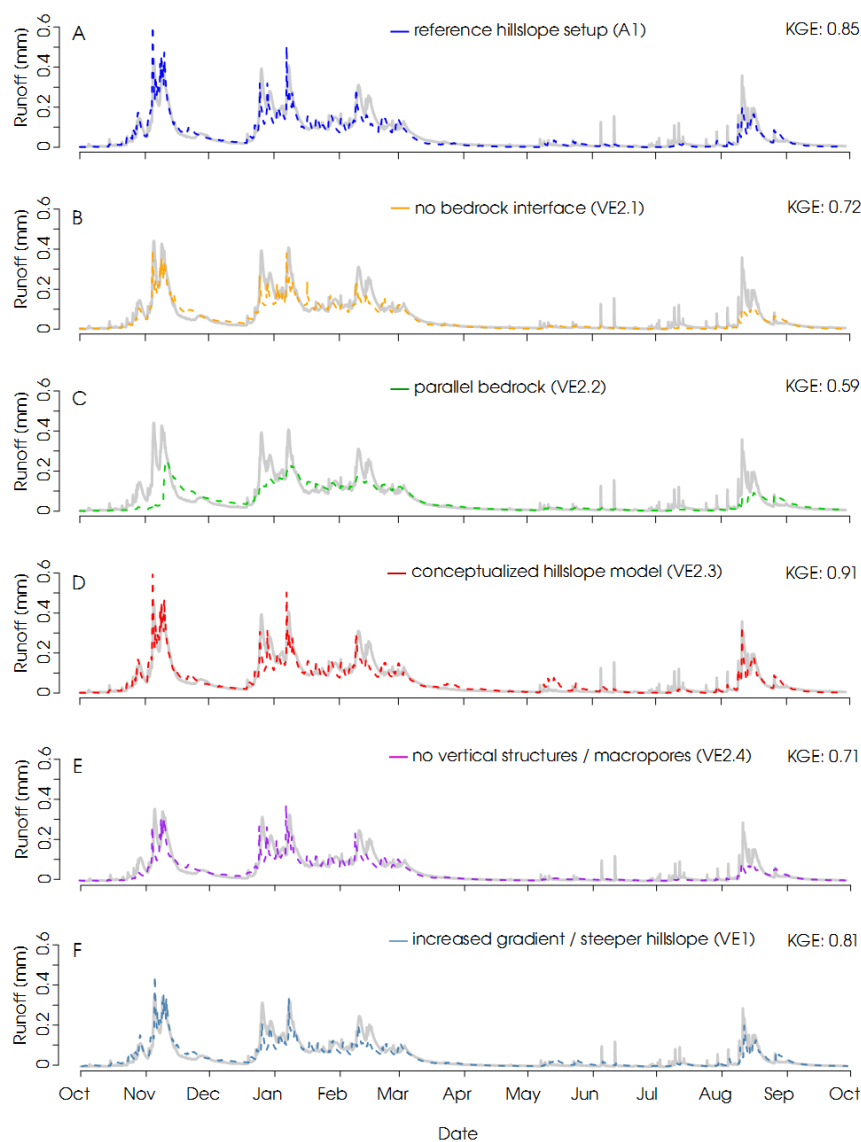


1364

1365 **Figure 10 (A) Normalized observed average sap velocities from 28 trees in the Colpach catchment against**
1366 **normalized simulated transpiration from the reference model as well as from the model with the improved**
1367 **transpiration routine; both were smoothed with a three day rolling mean. (B) Section of the Colpach reference**
1368 **model in the winter period (January) and in the vegetation period (June) with the relative saturation for every**
1369 **cell.**



1370



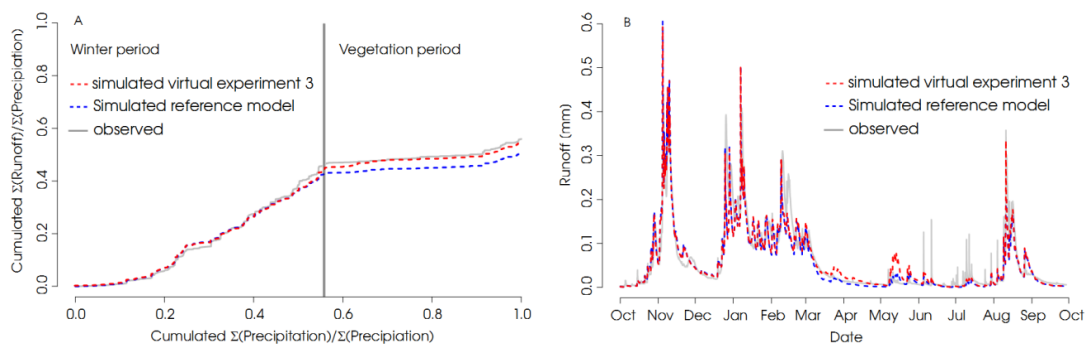
1371

1372 **Figure 11 Virtual experiment 2: (A) Simulated runoff from the reference model setup (A1), (B) model setup with**
1373 **no bedrock interface (VE2.1), (C) model setup with a parallel bedrock to the surface topography (VE2.2), (D)**
1374 **model setup with a conceptualized storage at the hill foot (VE2.3), (E) hillslope without vertical structures**
1375 **(VE2.4), (F) increased topographic gradient through a steeper hillslope topography (VE1)**

1376

1377

1378



1379

1380 **Figure 12 Virtual experiment 3: Normalized double mass curves (A) and discharge (B) from the model with the**
1381 **improved starting point of vegetation period (red), from the original model setup (blue) as well as the observed**
1382 **normalized double mass curve and runoff (grey).**

1383